



Geochemistry, Geophysics, Geosystems

RESEARCH ARTICLE

10.1029/2018GC007448

Key Points:

- Contrasting Nd isotope values of Cretaceous sediments in the eastern Central Atlantic Ocean
- Increasing contribution from inner Precambrian sources during the Late Cretaceous
- Three-step evolution of the West African Craton drainage areas during the Cretaceous

Supporting Information:

- Supporting Information S1
- Table S1
- Table S2
- Table S3

Correspondence to:

M. Roddaz,
martin.roddaz@get.omp.eu

Citation:

Mourlot, Y., Roddaz, M., Dera, G., Calvès, G., Kim, J.-H., Chaboureaud, A.-C., et al. (2018). Geochemical evidence for large-scale drainage reorganization in Northwest Africa during the Cretaceous. *Geochemistry, Geophysics, Geosystems*, 19, 1690–1712. <https://doi.org/10.1029/2018GC007448>

Received 22 JAN 2018

Accepted 21 APR 2018

Accepted article online 27 APR 2018

Published online 20 MAY 2018

Geochemical Evidence for Large-Scale Drainage Reorganization in Northwest Africa During the Cretaceous

Yannick Mourlot^{1,2} , Martin Roddaz¹ , Guillaume Dera¹ , G r me Calv s¹ , Jung-Hyun Kim³ , Anne-Claire Chaboureaud⁴, St phanie Mounic¹, and Fran ois Raison²

¹G osciences-Environnement Toulouse, Universit  de Toulouse, UPS (SVT-OMP), CNRS, IRD, Toulouse, France, ²Total E&P, CSTJF Avenue Larribau, Pau, France, ³Department of Geophysics, Korea Polar Research Institute, Incheon, South Korea, ⁴CVA Engineering 9/11, all e de l'Arche, Tour Eg e, Courbevoie, La D fense, France

Abstract West African drainage reorganization during Cretaceous opening of the Atlantic Ocean is deciphered here from geochemical provenance studies of Central Atlantic sediments. Changes in the geochemical signature of marine sediments are reflected in major and trace element concentrations and strontium-neodymium radiogenic isotopic compositions of Cretaceous sedimentary rocks from eight Deep Sea Drilling Project (DSDP) sites and one exploration well. Homogeneous major and trace element compositions over time indicate sources with average upper (continental) crust signatures. However, detailed information on the ages of these sources is revealed by neodymium isotopes (expressed as ϵNd). The $\epsilon\text{Nd}(0)$ values from the DSDP sites show a three-step decrease during the Late Cretaceous: (1) the Albian-Middle Cenomanian $\epsilon\text{Nd}(0)$ values are heterogeneous (-5.5 to -14.9) reflecting the existence of at least three subdrainage basins with distinct sedimentary sources (Hercynian/Paleozoic, Precambrian, and mixed Precambrian/Paleozoic); (2) during the Late Cenomanian-Turonian interval, $\epsilon\text{Nd}(0)$ values become homogeneous in the deep-water basin (-10.3 to -12.4), showing a negative shift of 2 epsilon units interpreted as an increasing contribution of Precambrian inputs; (3) this negative shift continues in the Campanian-Maastrichtian ($\epsilon\text{Nd}(0) = -15$), indicating that Precambrian sources became dominant. These provenance changes are hypothesized to be related to the opening of the South and Equatorial Atlantic Ocean, coincident with tectonic uplift of the continental margin triggered by Africa-Europe convergence. Finally, the difference between $\epsilon\text{Nd}(0)$ values of Cretaceous sediments from the Senegal continental shelf and from the deepwater basins suggests that ocean currents prevented detrital material from the Mauritanides reaching deepwater areas.

1. Introduction

Geodynamic cycles of several hundreds of million years, known as Wilson cycles (Wilson, 1968), have driven the accretion and breakup of continents and lithosphere since ~ 3 billion years ago (Ga; Shirey & Richardson, 2011). The stretching and thinning of continental lithosphere related to heat transfer in the mantle leads to magmatic activity and rifting, which can potentially evolve toward plate separation and the formation of oceanic crust (Dewey & Burke, 1974; Seng r & Burke, 1978). Conversely, plate convergence results in oceanic closure and continental collisions, which ultimately lead to the assembly of supercontinents (Dewey et al., 1986; Valentine & Moores, 1970). Due to their structural and metamorphic history, old and stable cratonic domains represent the archives of this geodynamic evolution because intra and pericratonic basins record the sedimentation and erosion associated with each cycle of divergence and convergence. The West African Craton (WAC, Figure 1a) is one of the best examples of sedimentary archives that reflect geodynamic events since it shows a continuous record of successive Wilson cycles since the Paleoproterozoic (Burke et al., 1976).

One way to reconstruct the denudation history of cratons is to determine the provenance of well-dated siliclastic sediments deposited in peripheral marginal basins. Any modification in clastic sediment sources will reflect changes in paleorelief, drainage configuration, as well as sediment transport associated with large-scale tectonic processes (e.g., Clift & Blusztajn, 2005). To supplement classic petrographic approaches based mainly on sand or coarser fractions (e.g., heavy mineral counting; Garzanti et al., 2007), geochemical provenance proxies are often used, these include major and trace elements (including rare earth element

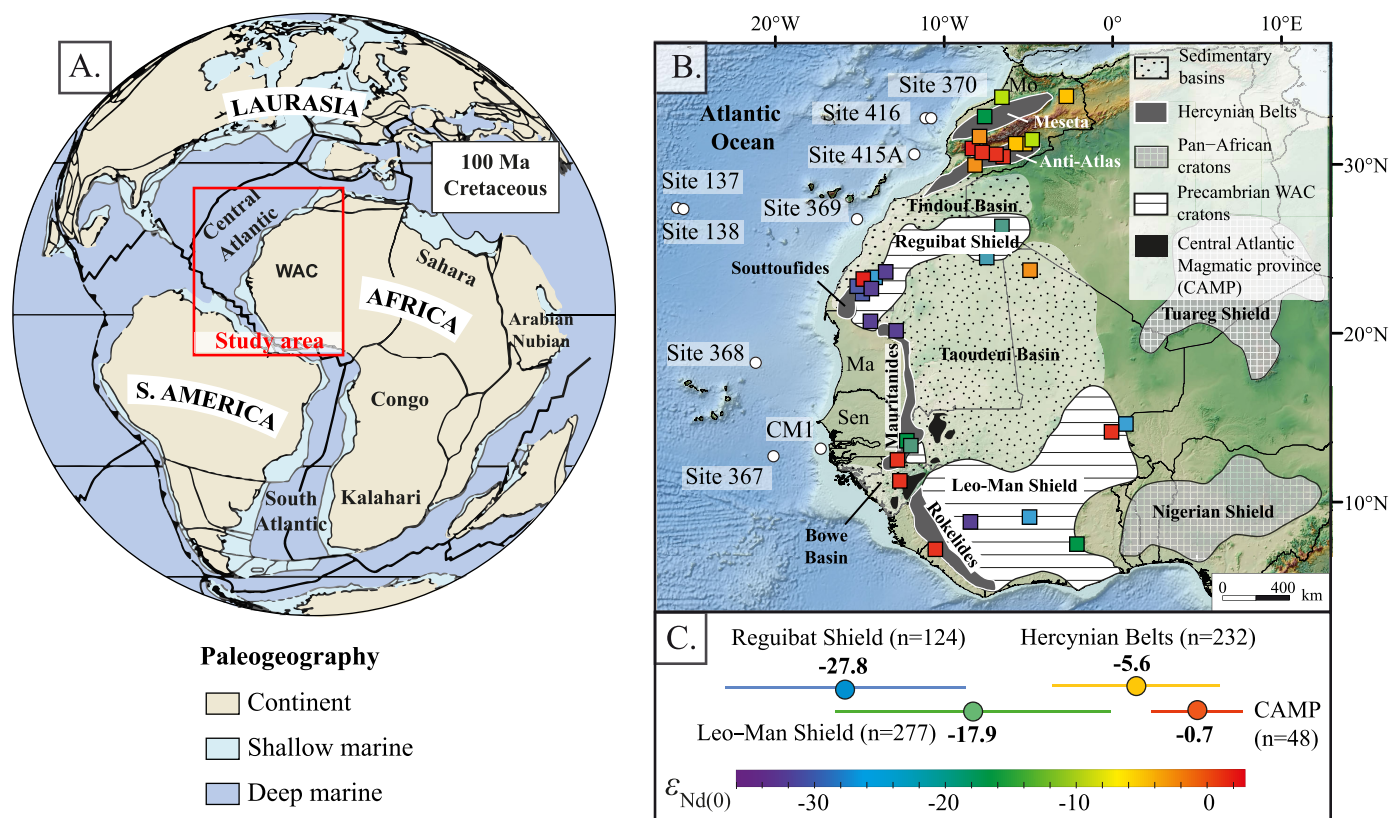


Figure 1. (a) Location of study area in its Cretaceous paleogeographical context (Torsvik et al. 2012). The red rectangle indicates position of area shown on Figure 1b. (b) Main geological units of the West African Craton (WAC) and location of studied boreholes including the exploration well CM1, DSDP leg 41 sites 367, 368, 369, 370, leg 50 sites 415A, 416, and leg 14 site 137 (white circles). Source ages are simplified from Milesi et al. (2010). Colored squares represent localities with published $\epsilon_{Nd(0)}$ data compiled in our database of potential sources. Colors indicate the average $\epsilon_{Nd(0)}$ values of sedimentary rocks for each locality (supporting information Table S1). (c) Averages and standard deviations of $\epsilon_{Nd(0)}$ values for the four main sources. The color-coded scale indicates the range of $\epsilon_{Nd(0)}$ values from radiogenic in red to very unradiogenic in purple. n refers to the total number of available values. Data from Hercynian orogenic belts include values from the Moroccan Meseta, Anti-Atlas and High-Atlas, as well as the Bassarides, Souttoudides, Mauritanides, and Rokelides. MO, Morocco; Sen, Senegal; Ma, Mauritania; CAMP, Central Atlantic Magmatic Province.

[REE] concentrations), uranium-lead (U-Pb) dating of detrital zircons and strontium (Sr)-neodymium (Nd) isotopic composition of detrital fractions. The results of these methods can be biased by the effect of grain-size/mineralogical sorting during transport and deposition that may control the geochemical composition of the sediments (Bouchez et al., 2011; McLennan et al., 1993; Roddaz et al., 2014). Despite the robustness of the U-Pb zircon dating method (Fedo et al., 2003), this mineral is usually extracted from medium-to-coarse grained sandstones, which are more sensitive to sedimentary sorting than fine-grained sediments (McLennan et al., 1993). By contrast, the Nd isotopic compositions of the sediment fine fraction ($<63 \mu\text{m}$) are not biased by grain-size sorting, allowing to establish a complete integration of drainage pathways from the most distant cratonic areas to oceanic basins (Goldstein et al., 1984; Patchett et al., 1999). This isotopic provenance approach may be suitable to determine the Cretaceous denudation history of the WAC because the lithogenic sediments are inherited from geological units with distinct radiogenic isotope signatures according to their age and composition (Boher et al., 1992; Deckart et al., 2005; Essaifi et al., 2014; Gasquet et al., 1992). Such a method has been successfully applied to trace the source of modern sediments deposited in the eastern Central Atlantic Ocean (Bayon et al., 2015; Grousset et al., 1998; Meyer et al., 2011). However, few studies have applied this method to characterize changes in sedimentary provenance during the major geodynamic events recorded in the WAC (Ali et al., 2014; Asiedu et al., 2005; Roddaz et al., 2007), especially during the Cretaceous phase of extension and opening of the Atlantic Ocean.

Here we determine the provenance of siliciclastic sediments deposited in the eastern Central Atlantic Ocean during the Cretaceous. Our study is based on major and trace element analyses and Sr-Nd isotopic data of

43 samples of clay-rich sedimentary rocks from eight DSDP sites along the Northwest African Margin and one exploration borehole (CM1, Figure 1b). We document major changes in the provenance of Atlantic sediments resulting from a large-scale reorganization of Northwest Africa drainage pathways during the Cretaceous.

2. Geological Setting and Sediment Sources

2.1. Geological Setting

The WAC consists of two Archaean and Paleoproterozoic shields, namely the Reguibat Shield to the North and the Leo-Man Shield to the South (Figure 1b), which were merged together (along with the Amazonian Craton) during the Paleoproterozoic Eburnean Orogeny (Ledru et al., 1994; Villeneuve & Cornée, 1994; Zhao et al., 2002). The earliest erosion of the WAC is recorded in the thick Precambrian sedimentary succession of the Taoudeni Basin, which separates the two shields (Milesi et al., 2010). Younger collision phases are also well identified on the craton borders (Figure 1b), corresponding to the Panafrican Orogeny toward the East which is a remnant of the Late Neoproterozoic to Early Cambrian collision with the Saharan and Congo cratons during the Gondwana assembly (Torsvik & Cocks, 2013, and references therein). Toward the West, the Hercynian Belts (represented by the Mauritanides, Souttoufides, Bassarides, Anti-Atlas, and Meseta chains) result from the formation of Pangea around 300 Ma (Drake, 1976; Villeneuve et al., 1993; Wegener, 1915). Associated with these episodes, the Tindouf Basin, the Bowe Basin, the Senegal-Mauritania Basin, and the internal parts of the Taoudeni Basin record the erosion of Paleozoic massifs (Figure 1b). Finally, the breakup of Pangea is characterized by a major episode of tholeiitic volcanism in the Central Atlantic Magmatic Province (CAMP) at 200 Ma (Marzoli et al., 1999; Olsen, 1999). This predates the opening of the Central Atlantic Ocean at ~185 Ma (Labails et al., 2010; Le Pichon, 1968; Torsvik et al., 2008), followed by the formation of the Equatorial Atlantic Ocean from 100 to 80 Ma (Binks & Fairhead, 1992; Sibuet & Mascle, 1978). These Mesozoic events, implying a long-wavelength extensional regime with compressive stress and vertical movements (Guiraud & Bosworth, 1997; Leprêtre et al., 2015), are associated with sedimentary deltas and deep-sea fan deposits corresponding to clastic supply from the WAC to the Northwest African Margin and the deepwater basin (Davison, 2005; Emery & Uchupi, 1984).

2.2. Sediment Sources

To characterize the sedimentary sources of the Cretaceous sediments deposited in the eastern Central Atlantic Ocean, we use a compilation of 794 published Sr and Nd isotope values measured on sedimentary and magmatic rocks of the WAC (supporting information Table S1, Ajaji et al., 1998; Ali et al., 2014; Allègre et al., 1981; Asiedu et al., 2005; Azzouni-Sekkal et al., 2003; Bea et al., 2013, 2015; Blanc et al., 1992; Boher et al., 1992; Deckart et al., 2005; Dia et al., 1997; D'Lemos et al., 2006; Dupuy et al., 1988; El Baghdadi et al., 2003; Ennih & Liégeois, 2008; Errami et al., 2009; Essaifi et al., 2014; Fullgraf et al., 2013; Gasquet et al., 1992, 2003; Jakubowicz et al., 2015; Key et al., 2008; Kouamelan et al., 1997; Le Goff et al., 2001; Meyer et al., 2011; Montero et al., 2014; Othman et al., 1984; Pawlig et al., 2006; Peucat et al., 2005; Potrel et al., 1998; Roddaz et al., 2007; Samson et al., 2004; Schaltegger et al., 1994; Schoepfer et al., 2015; Soumaila et al., 2008; Mohammed et al., 2015; Tahiri et al., 2010; Taylor et al., 1992; Thomas et al., 2002; Toummite et al., 2013; Verati et al., 2005). This database allows a comprehensive picture of differences in the isotopic composition of the main geological units present in the WAC (Figure 1c). Four end-members with characteristic Nd isotope signatures are defined according to age and geographical position. These include the Precambrian Reguibat Shield, the Precambrian Leo-Man Shield, the Paleozoic Hercynian domains, and the CAMP volcanic rocks, whose average $\epsilon_{\text{Nd}(0)}$ values and standard deviations correspond to -27.8 ± 9.2 , -17.9 ± 10.3 , -5.6 ± 6.5 , and -0.7 ± 3.6 , respectively. In comparison, modern Central Atlantic detritus yields $\epsilon_{\text{Nd}(0)}$ values between -16 and -12 (mean value: -13.8 ± 1.5). With the exception of the CAMP rocks, these potential sources display a great scattering of $^{87}\text{Sr}/^{86}\text{Sr}$ values (supporting information Table S1), meaning that these isotopic compositions are less useful to reconstruct sedimentary provenances in the WAC.

3. Materials and Methods

3.1. Sampling

Forty-three Cretaceous fine-grained sedimentary rocks (i.e., shales and claystones) were sampled from cores recovered at eight DSDP sites along the Northwest African Margin and from one exploration well

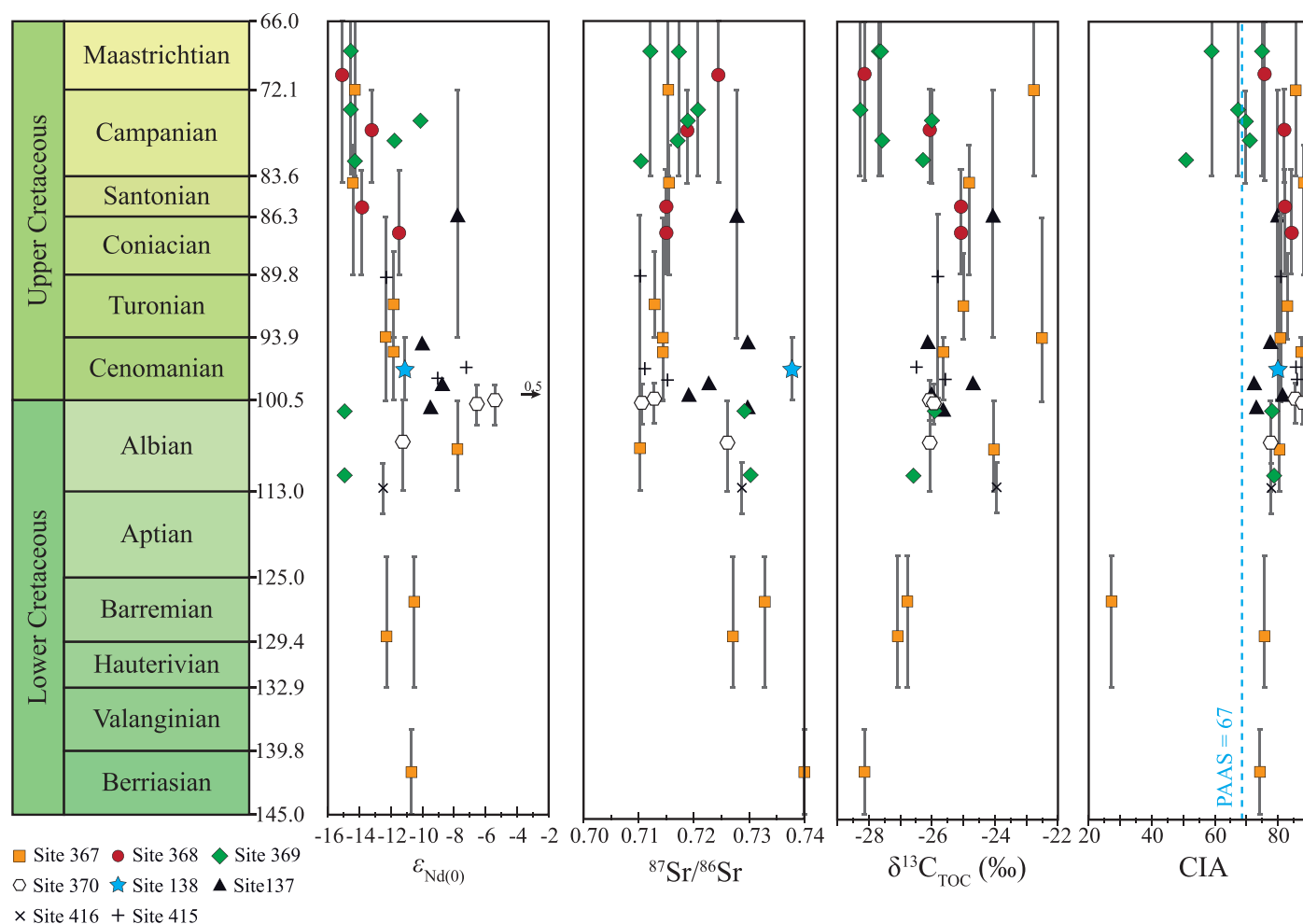


Figure 2. Stratigraphic framework, $\epsilon_{Nd(0)}$, $^{87}Sr/^{86}Sr$, $\delta^{13}C_{TOC}$, and CIA values of core samples from DSDP sites 367, 368, 369, 415A, 370, 137, 138, and 416 located in deepwater environments of the eastern Central Atlantic Ocean. Age uncertainties are indicated by grey vertical lines. Absence of a vertical line means that the uncertainty is less than the size of the symbol.

(Figure 1b). With the exception of well CM1 located on the continental shelf, the sedimentary rocks from the DSDP sites were deposited in deep pelagic environments occasionally influenced by distal turbidity currents (Jansa et al., 1978). Samples from DSDP sites were dated according to the biostratigraphical scheme defined for each DSDP site (Cepek, 1978; Cool et al., 2008; Foreman, 1978; Hayes et al., 1972; Lancelot et al., 1978; Lancelot & Winterer, 1980; Pflaumann & Čepek, 1982; Williams, 1978). The time resolution of samples is at the substage level (i.e., ~2 to 3 Ma) for the Late Albian-Turonian interval and at the stage level (i.e., ~5 to 10 Ma) for other intervals, which is sufficient to identify long-term trends in sedimentary provenance (Figure 2). To reassess the age of these samples, we compare their $\delta^{13}C_{TOC}$ values (Total Organic Carbon: TOC) against isotopic trends from the literature (Bodin et al., 2015; Friedrich et al., 2012). Eight shale samples from the Casamance-M – 1 exploration well (CM1, Figure 1b) were analyzed to obtain comparative data from a shelf paleoenvironment.

3.2. Bulk Organic Geochemical Analysis

The TOC contents of sediments and their stable carbon isotopic compositions ($\delta^{13}C_{TOC}$) were analyzed at the University of Hanyang (South Korea). Precisely weighed aliquots (0.5–16 g) of crushed and homogenized samples were decalcified by adding about 8 mL of 1 M HCl. After shaking overnight (~12 h) to remove carbonates prior to analysis, the TOC content and $\delta^{13}C_{TOC}$ values were determined by EA-IRMS (elemental analyzer-isotope ratio mass spectrometry, EuroEA-Isoprime IRMS, GV instruments, UK). The TOC content and isotope values were calibrated against a standard (IAEA-CH-6, TOC = 42.1%, $\delta^{13}C = -10.44\text{‰}$). The

analyses were performed at least in duplicate. The TOC data are given in weight percentage (wt %) and the $\delta^{13}\text{C}_{\text{TOC}}$ values are reported in the standard delta notation relative to the Vienna Pee Dee Belemnite (VPDB) standard. The analytical precision (as standard deviation for repeated measurements of the internal standard IAEA-CH-6, $n = 18$) is 1.1 wt % for TOC and 0.2‰ for $\delta^{13}\text{C}_{\text{TOC}}$.

3.3. Major and Trace Elements and Sr-Nd Isotopes

3.3.1. Sample Preparation

Each sample was finely crushed in an agate mortar. About 3 g of the crushed sediment were placed into 50 mL centrifuge tubes for sequential leaching to remove the nonterrigenous sedimentary components following the method of Bayon et al. (2002). Three different solutions composed of 5% acetic acid, 15% acetic acid and hydroxylamine hydrochloride (0.05 M), and hydrogen peroxide (H_2O_2 , 5%) were then added to remove the carbonates, Fe-Mn oxides and organic carbon, respectively. After the removal of nonterrigenous components, the residual fractions were cleaned with ultrapure water (MQ- H_2O , 18 M Ω). Clayey ($<2\ \mu\text{m}$) and silty (2–63 μm) fractions were then separated by centrifugation in two steps. First, 25 mL of MQ- H_2O was added to the detrital residues in the tubes, shaken vigorously, and then centrifuged for 2 min at 1,000 rpm (133 g). The clay-rich supernatants were immediately transferred into new 50 mL centrifuge tubes. Another 25 mL of MQ- H_2O was added to silt-rich detrital residues, mixed thoroughly again, centrifuged for 2.5 min at 800 rpm (85 g), and transferred into corresponding centrifuge tubes. Finally, clay-size fractions were collected after decantation (48 h) and centrifugation at 3,500 rpm (1,630g).

3.3.2. Major and Trace Element Analyses

The major and trace element concentrations were measured at the Service d'Analyse des Roches et Minéraux (SARM, INSU facility, Vandoeuvre-Les-Nancy, France) by ICP-OES (Na, Mg, K, Ca, Sc, Ti, Mn, Fe, Al, Si, and P) and ICP-MS (Rb, Cs, Ba, Sr, Th, U, Y, Zr, Nb, Hf, Cr, V, Co, Cu, Ni, Zn, La, Ce, Pr, Nd, Sm, Eu, Gd, Tb, Dy, Ho, Er, Tm, Yb, Lu, and Ta) after alkali fusion. Analytical details are available on <http://helium.crpq.cnrs-nancy.fr/SARM/> and in Carignan et al. (2001). Uncertainties are lower than 5% for elements measured by ICP-OES, and lower than 10% for elements measured by ICP-MS (see supporting information Table S2).

3.3.3. Nd-Sr Isotopes Compositions

The Nd-Sr isotopic compositions were measured at Géosciences Environnement Toulouse (GET) in France. About 100 mg of the leached detrital residue fractions were accurately weighted in cleaned Savillex PFA vials and then digested by several hot acid attacks. The analyzed fractions were firstly digested in hydrogen peroxide for 24 h at ambient temperature, and then digested in HNO_3 for 24 h at 80°C followed by HF-HNO_3 for 24 h at 80°C, and, finally $\text{HCl} + \text{HNO}_3$ for 24 h at 115°C. Blank tests were performed to estimate the level of contamination induced by the acid digestion, but it was found to be negligible. Aliquots containing about 1,000 ng of Sr and Nd were loaded into the ion exchange columns. Strontium and Nd were separated using the Sr-SPEC, TRU-SPEC and LN-SPEC resins (Eichrom). The isotopic values of both elements were measured using a Finnigan Mat 261 thermal ionization mass spectrometer and a Triton Thermal Ionization Mass Spectrometer in dynamic mode. During the Nd runs, a $^{146}\text{Nd}/^{144}\text{Nd}$ ratio of 0.7219 was used to correct the signal for mass fractionation. For each sample, checks were made for the absence of samarium (Sm). The accuracy of the measurements was estimated on the Université de Rennes 1 standard for Nd (0.511961 ± 14). This value was calibrated relative to the La Jolla standard by the Brest, Toulouse and Rennes laboratories (Lacan, 2002). During the Sr runs, $^{86}\text{Sr}/^{88}\text{Sr} = 0.1194$ was used to correct the signal for mass fractionation. The accuracy of the measurements was checked against the NBS 987 standard ($=0.710240$). The average values fall within the range given for these standards, so that no instrumental bias needs to be taken into account. Total blanks (acid digestion plus column chemistry) for Nd and Sr were checked by ICP-MS and found to be negligible compared to the Nd and Sr amounts loaded onto the columns. The measured $^{143}\text{Nd}/^{144}\text{Nd}_{\text{sample}}$ ratios are expressed in epsilon notation as the fractional deviation in parts per 10^4 (units) from $^{143}\text{Nd}/^{144}\text{Nd}$ value of the Chondritic Uniform Reservoir (CHUR). This notation is defined as

$$\varepsilon_{\text{Nd}(t)} = \left[\left(^{143}\text{Nd}/^{144}\text{Nd} \right)_{\text{sample}(t)} / \left(^{143}\text{Nd}/^{144}\text{Nd} \right)_{\text{CHUR}(t)} - 1 \right] \times 10^4$$

where t indicates the time at which ε_{Nd} is calculated. Here no time correction is applied ($t = 0$) and the $^{143}\text{Nd}/^{144}\text{Nd}_{\text{CHUR}(0)} = 0.512638$ (Jacobsen & Wasserburg, 1980).

4. Results

4.1. Organic Geochemistry and Stratigraphic Appraisal of $\delta^{13}\text{C}_{\text{TOC}}$ Data

The TOC results for the DSDP sites show a strong variability of values ranging from 0.07 to 11.84 wt % through the studied interval (Table 1). On average, samples from DSDP sites 367 and 369 appear to be more enriched in organic matter compared with other sites. By merging the $\delta^{13}\text{C}_{\text{TOC}}$ data from all DSDP sites, we observe a long-term trend, which can be correlated with recent compilations of NW Tethyan and Pacific $\delta^{13}\text{C}_{\text{bulk}}$ data showing characteristic patterns through the Cretaceous (Bodin et al., 2015; Friedrich et al., 2012). These literature data include (1) an increase of $\delta^{13}\text{C}_{\text{bulk}}$ values from the Berriasian to the Early Aptian; (2) a stepped long-term decrease from the Early Aptian to the Early Cenomanian; (3) a sharp positive Cenomanian excursion reaching a maximum at the Cenomanian-Turonian boundary; (4) a high isotopic plateau during the Turonian-Santonian interval; (5) a rapid decrease during the Campanian; and (6) a positive

Table 1

Organic Matter Contents and Stable Carbon Isotope Values (TOC and $\delta^{13}\text{C}_{\text{TOC}}$) of Sedimentary Rocks Analyzed in This Study

Leg-site-core	Age	$\delta^{13}\text{C}_{\text{TOC}}$ (‰ VPDB)	$\delta^{13}\text{C}$ STD	TOC (wt %)	TOC STD
14–137-6	Turonian-Campanian	−24.1	0.9	0.1	0.1
14–137-8	Late Cenomanian	−26.2	0.6	1.0	0.1
14–137-13	Early Cenomanian	−24.7	1.2	0.3	0.0
14–137-14	Early Cenomanian	−26.0	0.1	0.1	0.0
14–137-16	Late Albian	−25.6	0.5	3.1	0.1
41–367-15	Late Cretaceous-Paleogene (Campanian-Maastrichtian?)	−22.8	0.2	0.3	0.0
41–367-16	No older than Turonian	−24.8	0.7	0.2	0.0
41–367-17	No older than Turonian	−25.1	0.7	1.1	0.0
41–367-18	Late Cenomanian-Early Turonian	−22.5	1.4	5.2	0.1
41–367-19	Late to Middle Cenomanian	−25.7	0.6	10.0	0.1
41–367-23	Albian	−24.0	0.2	0.7	0.4
41–367-26	Early Aptian to Hauterivian	−26.7	0.2	1.3	0.1
41–367-27	Early Aptian to Hauterivian	−27.1	0.6	2.6	0.3
41–367-31	Early Valanginian to Berriasian	−28.1	0.2	2.2	0.1
41–368-53	Late Cretaceous (und., not older than Campanian?)	−26.3	0.5	0.1	0.0
41–368-55-2	Late Cretaceous (und., Campanian?)	−26.1	0.8	0.2	0.2
41–368-56	Late Cretaceous (und., younger than Turonian)	−25.1	0.9	0.2	0.1
41–368-57	Late Cretaceous (und., younger than Turonian)	−25.1	0.9	0.2	0.1
41–369-A38	Campanian-Maastrichtian	−27.6	0.2	0.5	0.0
41–369-38F	Campanian-Maastrichtian	−27.7	0.3	0.6	0.1
41–369-39	Campanian	−28.3	0.7	0.5	0.0
41–369-A40	Campanian	−26.0	0.7	0.4	0.0
369-41-1	Campanian	−27.6	0.0	11.8	0.8
41–369-41-3	Campanian	−26.2	0.7	6.7	1.7
41–369-43	Late Albian	−25.9	0.9	4.5	0.1
41–369-47	Early Albian	−26.6	0.7	2.6	0.1
41–370-20	Late Albian-Early Cenomanian	−26.0	0.8	0.7	0.1
41–370-22	Late Albian-Early Cenomanian	−25.9	0.7	0.9	0.1
41–370-27	Albian	−26.1	0.5	4.9	0.3
50–415-7	Cenomanian-Coniacian	−25.8	0.6	0.2	0.0
50–415-9	Middle Cenomanian	−26.5	1.2	1.6	0.2
50–415-13	Early Cenomanian	−25.7	0.9	0.9	0.2
50–416-6	Late Aptian-Early Albian	−23.9	0.4	0.4	0.0
CM1–9	Santonian-Early Campanian (probable)	−26.2		0.4	
CM1–7	Late Cenomanian-Early Turonian	−25.1		0.8	
CM1–6	Late Cenomanian-Early Turonian	−26.1		1.3	
CM1–5	Late Cenomanian-Early Turonian	−27.9		0.5	
CM1–4	Late to Middle Cenomanian	−27.6		0.1	
CM1–3	Early Cenomanian to Middle/Late Ceno.	−27.2		0.2	
CM1–2	Middle Albian	−25.5		0.1	
CM1-1	Early Aptian	−24.0		0.4	

Note. STD for standard deviation.

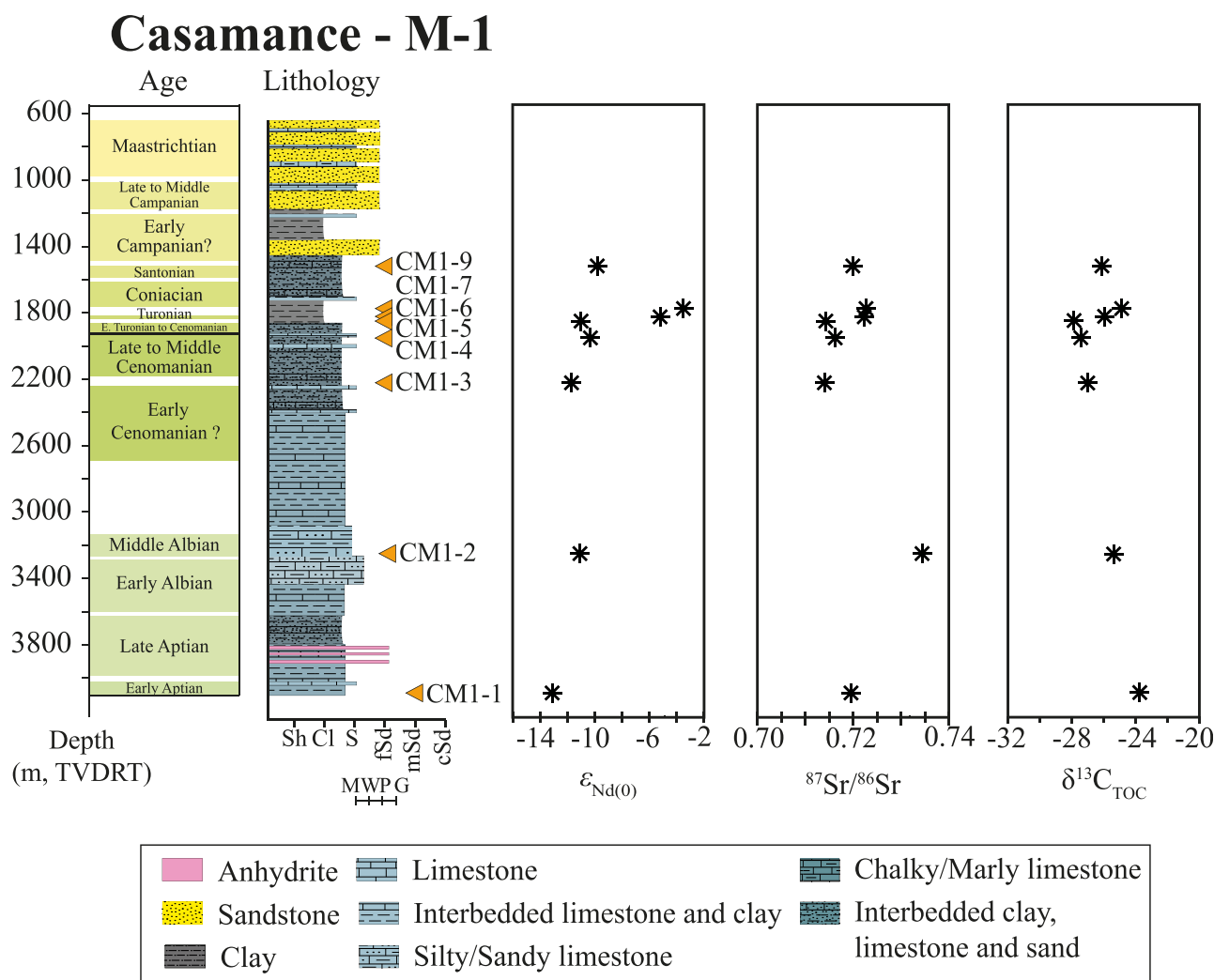


Figure 3. Stratigraphic framework, lithology, $\epsilon_{Nd(0)}$, $^{87}Sr/^{86}Sr$, and $\delta^{13}C_{TOC}$ values of Cretaceous sediments from the CM-1 well on the Casamance continental shelf. M, mudstone; W, wackestone; P, packstone; G, grainstone; Sh, shale; Cl, clay; S, silt; fSd, fine sandstone; mSd, medium sandstone; cSd, coarse sandstone.

excursion during the Maastrichtian. Our data fit relatively well with this long-term evolution since the analyzed $\delta^{13}C_{TOC}$ values record a progressive rise of $\delta^{13}C_{TOC}$ values from -28.1‰ to -22.5‰ during the Berriasian-Turonian interval, followed by relatively stable values up to the Santonian, and an abrupt decrease reaching a minimum of -28.3‰ at the Campanian-Maastrichtian boundary (Figure 2). The lack of positive carbon isotope excursion in the younger Cretaceous samples may exclude any Maastrichtian age from our study, except for one sample (namely 41–367-15) which has a distinct $\delta^{13}C_{TOC}$ value of -22.8‰ . Although the scarcity of $\delta^{13}C_{TOC}$ values from CM1 makes it more difficult to compare the data (Figure 3), the progressive decrease of -4‰ recorded within the Early Aptian-Early Cenomanian interval and the rapid positive excursion of 3.5‰ observed at the Cenomanian-Turonian boundary are in agreement with previously reported findings (Bodin et al., 2015; Friedrich et al., 2012).

4.2. Major Elements, Large-Ion Lithophile Elements (LILEs), High Field Strength Elements (HFSEs), and Trace Transition Elements (TTEs)

Figure 4 shows the elemental concentrations of major elements, LILE, HFSE, and TTE of samples normalized to the Post Archean Australian Shales (PAAS) concentration (Taylor & McLennan, 1985). As a whole, the elemental composition of the analyzed shales is rather uniform and close to PAAS values. No apparent trend of major depletion or enrichment in elemental concentration is recorded whatever the location of the DSDP site or the age of sediments.

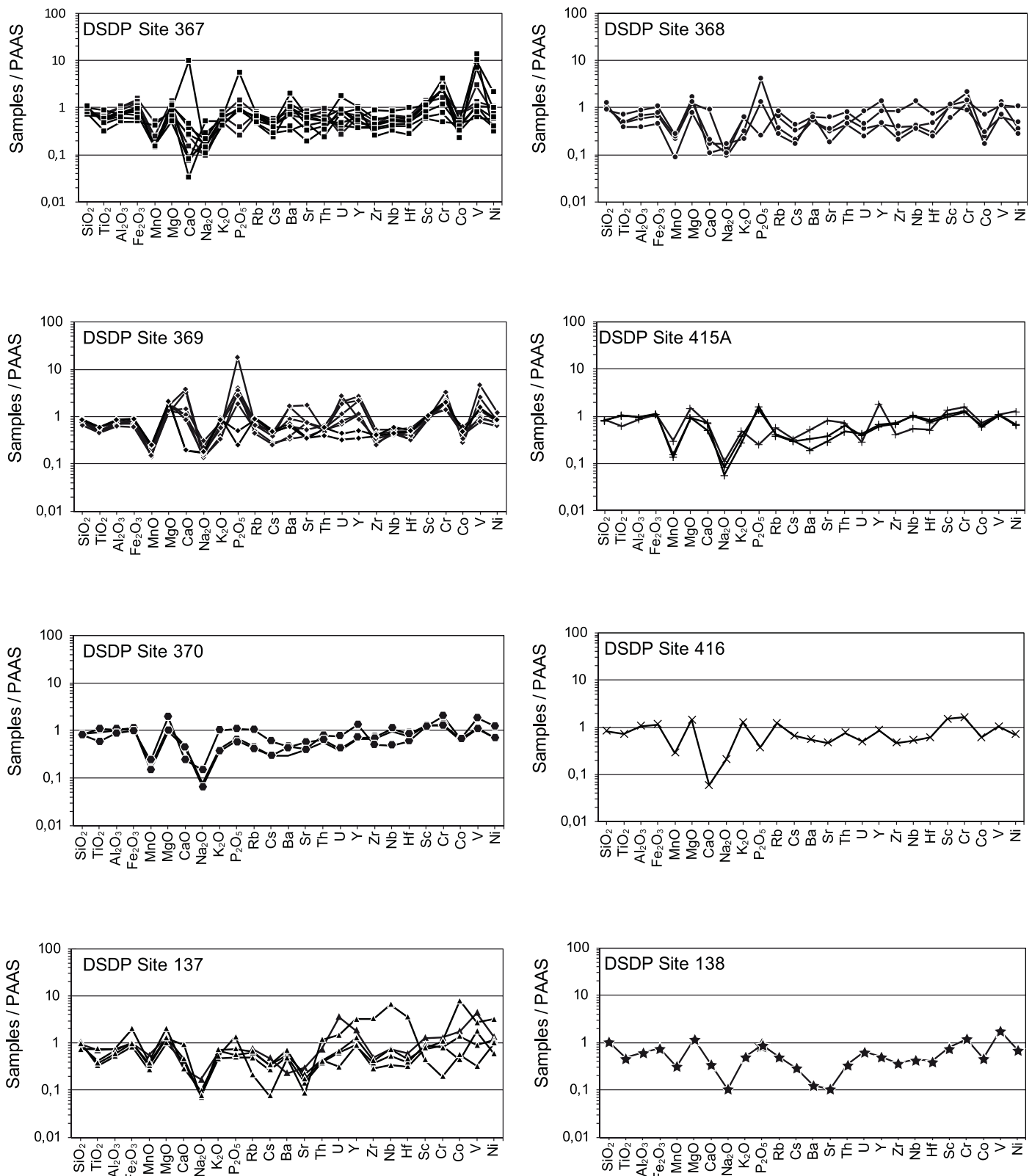


Figure 4. Major and selected trace element contents normalized to (Taylor & McLennan, 1985). From left to right on the diagram, the major elements (SiO₂, TiO₂, Al₂O₃, Fe₂O₃, MnO, MgO, CaO, Na₂O, K₂O, and P₂O₅), LILE (Rb, Cs, Ba, Sr, Th, and U), HFSE (Y, Zr, Nb, and Hf), and TTE (Sc, Cr, Co, V, and Ni) are plotted for DSDP sites 367, 368, 369, 370, 137, 415A, and 416.

It is possible to assess the degree of source-area weathering and the paleoweathering conditions of ancient sediments using the Chemical Index of Alteration (CIA; Fedo et al., 1995; Nesbitt & Young, 1982; Figure 2). This index measures the weathering intensity of feldspars relative to unaltered protoliths, and is defined as $CIA = [Al_2O_3 / (Al_2O_3 + CaO^* + Na_2O + K_2O)] \times 100$ (in molar proportions), where CaO^* represents the CaO content in the silicate fraction. CIA values for unaltered plagioclase and K-feldspars typical of unaltered upper crustal rocks are approximately equal to 50, whereas higher CIA values represent higher degrees of weathering. For comparison, the CIA value of the PAAS standard, which is representative of the upper continental crust composition, is equal to 67 (Taylor & McLennan, 1985).

Compared with PAAS, the DSDP site samples have higher CIA values (70–86) typical of intense weathering, with the exception of four samples (i.e., 41–367-26, 41–369-41-3, 41–369-39, and 41–369-38F, Table 2) whose CaO contents (1.9–12.7) are also higher than in PAAS (Table 2 and Figure 4). With the exception of one sample (14–137-14, Early Cenomanian), the analyzed DSDP site samples have higher Cr/Th ratios (11.2–62) and lower Th/Sc ratios (0.3–0.8) than PAAS (Table 2). The Early Cenomanian sample 14–137-14 has a lower Cr/Th ratio (1.3) and much higher Th/Sc ratio (2.5) in comparison with PAAS (Table 2). At each DSDP site, there is no apparent variation of these ratios (CIA, Th/Sc , and Cr/Th) as a function of the age of the sample (Table 2).

4.3. Rare Earth Elements (REEs)

To facilitate comparisons with sediments derived from basic or felsic sources (Cullers, 2000) and the PAAS (Taylor & McLennan, 1985), the Eu anomaly is calculated with respect to chondrites: $Eu/Eu^* = Eu_N / (Sm_N \times Gd_N)^{1/2}$ where N refers to the chondrite-normalized concentration value (Condie, 1993). The cerium anomaly (ΩCe) normalized to PAAS is calculated following De Baar et al. (1985): $\Omega Ce = 2 \times (Ce_{sample}/Ce_{PAAS}) / [(La_{sample}/La_{PAAS}) + (Pr_{sample}/Pr_{PAAS})]$, where X_{sample} is the concentration of samples and X_{PAAS} refers to the concentrations of the PAAS standard (Taylor & McLennan, 1985).

With the exception of the Early Cenomanian sample 14–137-14, the analyzed core samples from DSDP sites have flat REE patterns typical of shales (Figure 5). Their Eu/Eu^* ratios are slightly higher (0.69–0.87) compared to the PAAS standard (i.e., $Eu/Eu^* = 0.66$) and their Ce anomalies display variable values (0.66–1.13) around the PAAS standard (i.e., $\Omega Ce = 1$) (Table 2). Despite the wide range of variation of cerium anomalies, the values are systematically higher than those measured in authigenic smectites and seawater ($\Omega Ce < 0.50$; De Baar et al., 1985). The Eu and Ce anomalies do not show any variation with stratigraphic position. Only the Early Cenomanian sample 14–137-14 is enriched in HREE compared to PAAS and shows a low Eu/Eu^* ratio (0.46, Figure 5 and Table 2).

4.4. Sr-Nd Isotopes

Table 3 reports the Sr-Nd isotopic compositions of samples analyzed in this study. Overall, the $^{87}Sr/^{86}Sr$ ratios of DSDP samples show a progressive decrease from 0.740 to ~ 0.730 through the Early Cretaceous, a net drop at the Albian-Cenomanian boundary, and relatively stable values (~ 0.715) during the Late Cretaceous (Figure 2). With the exception of the DSDP 137 site, all the DSDP samples show an overall lowering of their $\epsilon_{Nd(0)}$ values throughout the Cretaceous. If we exclude the few data points obtained for the Berriasian to Barremian interval, three steps can be observed in the evolution during the rest of the Cretaceous (Figure 2): (1) The $\epsilon_{Nd(0)}$ values are highly variable and generally more radiogenic in the Albian-Middle Cenomanian (–15 to –5.5); (2) they become homogeneous and close to –11 in the Late Cenomanian-Turonian; and (3) the $\epsilon_{Nd(0)}$ values become systematically more negative (i.e., between –14.3 and –15) in the youngest Campanian-Maastrichtian samples (Table 3). With the exception of the Early Cenomanian sample (sample 14–137-14), which yields a positive $\epsilon_{Nd(0)}$ value (+0.5), samples from the DSDP site 137 show an opposite trend with the uppermost Turonian-Campanian sample having the least negative value $\epsilon_{Nd(0)}$ value (sample 14–137-6, $\epsilon_{Nd(0)} \sim -7.7$). Overall, two trends can be observed in the $\epsilon_{Nd(0)}$ variations recorded on the continental shelf (CM1 well; Figure 3). The Early Aptian to Early Turonian samples (CM1 – 1 to CM1 – 5) show a slight increase of 2.5 epsilon units through time. The two youngest samples of the Late Cenomanian-Early Turonian (CM1 – 6 and CM1 – 7) have significantly more radiogenic $\epsilon_{Nd(0)}$ values (–3.6 and –5.1). These two samples also yield higher $^{87}Sr/^{86}Sr$ values.

Table 2
Major and Trace Element Concentrations of Sedimentary Rocks Analyzed in This Study

Leg-site- core	14- 137-6	14- 137-8	14- 137-13	14- 137-14	14- 137-16	14- 138-6	41- 367-15	41- 367-16	41- 367-17	41- 367-18	41- 367-19	41- 367-20	41- 367-23	41- 367-26	41- 367-27	41- 367-31	41- 368-53	41- 368-55-2
SiO ₂ (wt %)	58.84	68.84	58.27	46.41	61.57	66.96	48.25	50.32	50.65	56.80	50.47	43.78	62.44	49.18	60.03	66.79	66.34	62.76
Al ₂ O ₃ (wt %)	13.91	9.77	13.10	14.00	11.01	11.76	19.96	19.79	16.52	12.48	14.85	14.83	13.85	9.44	13.89	11.58	10.94	12.99
Fe ₂ O ₃ (wt %)	6.40	5.46	6.80	12.99	6.40	4.97	9.83	8.52	8.44	7.09	5.29	6.80	6.09	3.23	4.53	3.82	4.26	4.96
MnO (wt %)	0.06	0.02	0.03	0.04	0.04	0.03	0.05	0.02	0.03	0.02	0.00	0.02	0.02	0.05	0.02	0.00	0.02	0.03
MgO (wt %)	2.92	2.21	2.80	4.50	2.85	2.60	1.71	1.71	2.99	1.96	2.05	1.52	1.11	1.91	2.60	2.39	2.69	3.65
CaO (wt %)	0.37	0.52	1.20	0.37	0.59	0.44	0.19	0.33	0.09	0.04	0.11	0.34	0.10	12.71	0.48	0.59	1.15	0.14
Na ₂ O (wt %)	0.20	0.09	0.08	0.11	0.09	0.12	0.12	0.11	0.29	0.34	0.20	0.20	0.61	0.13	0.25	0.17	0.11	0.17
K ₂ O (wt %)	2.37	1.75	2.55	1.97	2.68	1.84	2.49	1.82	2.52	2.17	1.62	2.36	1.92	1.55	2.91	2.50	1.13	2.22
TiO ₂ (wt %)	0.71	0.33	0.41	0.75	0.37	0.49	0.74	0.67	0.58	0.54	0.57	0.62	0.87	0.31	0.57	0.46	0.48	0.49
P ₂ O ₅ (wt %)	0.00	0.08	0.09	0.22	0.12	0.14	0.06	0.04	0.23	0.16	0.14	0.88	0.00	0.16	0.00	0.14	0.65	0.00
LOI	13.86	10.19	13.96	18.90	12.96	11.01	15.33	16.65	18.35	19.17	24.70	28.60	14.18	21.01	15.09	12.02	13.22	13.23
Total	99.66	99.29	99.35	100.28	98.70	100.38	98.75	99.98	100.70	100.77	100.02	99.96	101.20	99.67	100.36	100.45	100.98	100.65
Al/Si	0.27	0.16	0.26	0.34	0.20	0.20	0.47	0.45	0.37	0.25	0.33	0.38	0.25	0.22	0.26	0.20	0.19	0.23
Cl/Al	80	77	72	82	73	80	86	88	83	81	87	81	81	27	76	74	76	82
Sc (ppm)	20.47	12.02	14.62	7.00	12.65	12.67	22.96	21.32	20.27	15.51	17.98	17.38	17.95	9.20	12.87	9.99	18.26	16.92
Rb (ppm)	120.50	77.59	99.61	33.43	105.80	81.68	121.90	110.20	121.80	93.99	83.54	126.85	74.35	76.48	118.70	104.06	59.35	102.20
Cs (ppm)	7.20	4.05	5.10	1.13	5.13	4.28	6.45	6.46	8.51	6.73	6.24	7.46	3.54	4.33	6.66	5.82	3.15	4.79
Ba (ppm)	149.50	329.20	366.80	314.03	463.70	81.21	456.60	515.40	547.00	1,302.00	792.26	694.74	672.47	213.64	452.04	253.29	335.00	341.00
Sr (ppm)	59.77	28.63	44.09	17.07	34.36	20.75	115.90	139.00	165.70	133.00	143.64	84.95	118.18	89.98	64.86	38.05	61.64	69.83
Th (ppm)	10.81	5.60	6.49	17.22	6.08	5.14	13.02	11.30	13.81	7.67	8.99	7.27	7.57	3.44	6.02	4.95	6.29	8.60
U (ppm)	11.11	1.92	0.95	4.59	2.11	2.02	0.98	0.83	2.44	1.28	2.90	5.31	2.28	2.81	2.53	1.11	2.53	1.11
Y (ppm)	50.03	24.88	23.73	86.39	34.61	13.82	22.53	17.26	18.91	9.99	12.50	28.04	16.74	25.46	10.05	14.45	37.28	11.69
Zr (ppm)	103.00	60.08	79.42	695.82	88.54	74.87	107.00	92.60	98.06	79.54	92.45	120.54	183.64	52.53	89.84	72.70	56.76	82.43
Nb (ppm)	3.01	1.59	1.96	18.00	2.28	2.07	3.16	2.70	2.74	2.31	2.51	3.00	4.84	1.37	2.51	1.98	1.45	2.36
Hf (ppm)	142.50	97.94	87.37	21.50	119.50	129.60	216.60	244.60	176.60	278.60	272.84	452.50	284.17	54.09	127.52	82.57	231.30	96.16
V (ppm)	658.80	269.10	135.60	48.95	413.90	268.30	198.80	164.20	439.40	205.50	1,044.56	1,489.81	165.42	92.88	157.12	118.88	195.40	94.65
Co (ppm)	40.91	10.20	31.95	13.07	184.10	10.75	17.19	17.34	10.27	5.08	6.98	12.34	9.62	10.72	9.20	7.28	5.50	6.87
Ni (ppm)	153.80	41.01	130.80	17.65	149.80	52.64	26.83	35.39	150.80	131.50	150.59	93.57	32.67	50.82	54.03	40.17	27.12	24.01
Cu (ppm)	72.89	32.29	63.64	54.79	177.20	38.81	58.51	56.06	43.32	17.10	53.06	117.21	21.84	31.04	33.72	21.73	19.64	26.78
Zn (ppm)	149.80	82.34	82.19	115.30	203.50	71.63	123.00	129.30	130.60	57.71	153.88	437.42	39.87	41.37	75.83	65.79	101.00	81.38
La (ppm)	49.59	25.98	22.61	57.70	36.32	17.38	37.46	31.99	35.02	19.13	22.99	32.84	31.60	22.23	21.08	18.21	57.26	20.65
Ce (ppm)	120.90	41.34	38.91	97.03	66.76	28.90	89.82	63.49	60.34	29.54	37.98	52.61	63.93	36.20	38.18	33.15	112.40	46.75
Pr (ppm)	13.24	6.60	6.49	11.83	9.46	3.78	8.90	6.84	6.34	3.41	4.31	7.52	6.99	5.56	4.48	4.56	12.93	5.08
Nd (ppm)	52.06	25.18	26.19	44.14	37.22	14.30	32.17	24.53	22.35	11.38	15.41	29.08	25.81	23.19	16.58	18.65	47.30	18.36
Sm (ppm)	11.16	5.04	5.55	10.16	7.55	2.79	6.11	4.68	4.09	1.89	2.96	5.63	4.93	4.91	3.09	3.82	8.79	3.61
Eu (ppm)	2.50	1.16	1.27	1.53	1.60	0.62	1.39	1.06	0.87	0.39	0.62	1.29	1.13	1.14	0.62	0.80	2.32	0.77
Gd (ppm)	9.89	4.37	4.83	10.10	6.69	2.36	4.99	3.68	3.24	1.54	2.29	4.81	3.81	4.60	2.27	3.22	7.62	2.76
Tb (ppm)	1.50	0.66	0.69	1.84	0.98	0.34	0.74	0.55	0.48	0.22	0.34	0.71	0.54	0.66	0.32	0.43	1.12	0.41
Dy (ppm)	9.06	3.98	4.02	12.89	5.73	2.16	4.32	3.20	2.99	1.39	2.17	4.36	3.22	3.84	1.81	2.42	6.62	2.41
Ho (ppm)	1.89	0.82	0.82	2.88	1.16	0.45	0.87	0.65	0.65	0.31	0.46	0.93	0.65	0.79	0.39	0.49	1.31	0.48
Er (ppm)	4.84	2.13	2.07	8.06	2.94	1.23	2.27	1.74	1.83	0.92	1.36	2.56	1.73	1.95	1.08	1.25	3.24	1.26
Tm (ppm)	0.64	0.30	0.27	1.11	0.40	0.19	0.32	0.26	0.28	0.15	0.21	0.37	0.25	0.26	0.16	0.17	0.42	0.19
Yb (ppm)	4.08	1.85	1.78	6.94	2.49	1.29	2.15	1.75	2.01	1.11	1.58	2.61	1.65	1.65	1.13	1.12	2.42	1.30
Lu (ppm)	0.59	0.28	0.26	0.97	0.36	0.20	0.33	0.27	0.32	0.18	0.25	0.42	0.27	0.25	0.19	0.18	0.34	0.21
Ta (ppm)	1.23	0.51	0.71	11.77	1.04	0.69	1.15	1.09	0.92	0.70	0.88	0.97	1.26	0.53	0.81	0.63	0.58	0.72
Eu/Eu*	0.73	0.76	0.75	0.46	0.69	0.74	0.76	0.78	0.73	0.70	0.74	0.76	0.79	0.73	0.72	0.70	0.87	0.74
ΩCe	1.08	0.72	0.73	0.85	0.83	0.82	1.13	0.99	0.92	0.83	0.87	0.77	0.99	0.75	0.90	0.84	0.95	1.01
Cr/Th	13.2	17.5	13.5	19.6	13.3	25.2	16.6	21.7	12.8	36.3	30.3	62.3	15.7	21.2	16.7	36.8	11.2	11.2
Th/Sc	0.53	0.47	0.44	2.46	0.48	0.41	0.57	0.53	0.68	0.49	0.50	0.42	0.42	0.37	0.47	0.50	0.34	0.51
Zr/Sc	5.0	5.0	5.4	99.4	7.0	5.9	4.7	4.3	4.8	5.1	5.1	6.9	10.2	5.7	7.0	7.3	3.1	4.9
LREE	4.42	2.21	2.14	4.23	3.18	1.33	2.99	2.38	2.33	1.24	1.57	2.62	2.42	1.93	1.58	1.57	4.44	1.69
HREE	4.46	2.05	1.94	7.53	2.74	1.41	2.34	1.90	2.19	1.19	1.69	2.84	1.82	1.80	1.25	1.24	2.69	1.43

Table 2. (continued)

[illegible]

Note. Uncertainties for all elements are given in the supporting information Table S2. $LREE = La_{PAAS} + Pr_{PAAS} + Nd_{PAAS} + Tb_{PAAS} + Dy_{PAAS}$ (in ppm); $HREE = Tm_{PAAS} + Yb_{PAAS} + Lu_{PAAS}$ (in ppm); $MREE^* = (HREE + LREE)/2$; $CIA = [Al_2O_3/(Al_2O_3 + CaO^* + Na_2O + K_2O) \times 100]$ (in molar proportions); $Eu/Eu^* = Eu_N/(Sm_N \times Gd_N)^{1/2}$ where X_N refers to the chondrite-normalized concentration value (Condie, 1993); $QCe = 2 \times (Ce_{sample}/La_{PAAS}) + (Pr_{sample}/Pr_{PAAS})$.

5. Discussion

5.1. Influence of Chemical Weathering and Marine Authigenesis on Provenance Proxies

The REE contents, Eu anomaly, elemental ratios (Cr/Th and Th/Sc) and Sr-Nd isotopic compositions of sedimentary rocks prove to be useful tools for determining the provenance of sediments (McLennan et al., 1993). However, before drawing conclusions on provenance, the effects of chemical weathering and marine authigenesis should be carefully assessed as these processes may control the REE contents and radiogenic isotope composition of marine sediments. Despite the fact that individual samples have variable and high CIA values (Table 2 and Figure 2), the absence of any correlation with REE content, Eu/Eu*, Cr/Th, Th/Sc, Sr, and Nd isotopes (see supporting information Table S3) suggests that chemical weathering has not modified these provenance proxies. Any influence from carbonates, Fe-Mn oxides or organic matter formed under marine conditions may also be ruled out since these constituents are removed by the sequential leaching steps. Moreover, the REE patterns of authigenic smectites formed in deepwater environments are normally characterized by LREE depletion, HREE enrichment and strong negative Ce anomalies ($\Omega_{Ce} < 0.50$; De Baar et al., 1985) typical of seawater (Piper, 1974). Here all the analyzed DSDP samples have Ce anomalies higher than or equal to 0.66. This suggests that, even if authigenic smectites were incorporated during early diagenetic processes, their proportion was much less than the detrital fraction. Rare earth element abundance patterns support this conclusion, with the exception of one sample from DSDP site 137 situated close to the mid-oceanic ridge (Figure 1b), since all the other analyzed samples (Figure 6) plot outside the seawater field, suggesting a negligible influence of marine authigenesis. The Early Cenomanian sample from DSDP site 137 (sample 14–137-14) plots in the seawater field, and is therefore considered as strongly affected by marine authigenesis. This sample is not taken into account for the provenance interpretations.

High Eu anomalies and Th/Sc ratios are characteristic of felsic and more highly differentiated source rocks, whereas high Cr/Th and low Eu anomalies suggest more mafic and less differentiated source rocks (e.g., Cullers, 2000; McLennan et al., 1993). Here the samples from the DSDP and CM1 sites have higher Cr/Th, but lower Th/Sc values and Eu anomalies compared to PAAS (Table 2). This suggests that the detrital supply came from less differentiated sources than those of PAAS, the latter being considered as representative of the Upper Continental Crust (Taylor & McLennan, 1985). If we exclude the diagenetically altered Early Cenomanian sample from DSDP site 137, no temporal or spatial variations are observed in CIA values, Eu and Ce anomalies or in the elemental ratios used for provenance studies (Cr/Th and Th/Sc; Figures 4 and 5 and Table 2). Only the $\epsilon_{Nd(0)}$ and $^{87}Sr/^{86}Sr$ values are found to vary through time, with $\epsilon_{Nd(0)}$ during the Late Cretaceous with a trend toward lower $\epsilon_{Nd(0)}$ values reflecting increasing inputs from older continental crust during the Late Cretaceous (Figure 2). Hence, this $\epsilon_{Nd(0)}$ value decrease reflects a progressive shift in the average age of source rocks rather than changes in the nature of the source (felsic as against basic). When plotted in a $^{87}Sr/^{86}Sr$ vs. $\epsilon_{Nd(0)}$ diagram and compared with relevant source fields (Precambrian, Hercynian/Paleozoic and CAMP sources) and with present-day Central Atlantic Ocean sediments (Figure 7), the Sr-Nd isotopic compositions of analyzed Cretaceous sedimentary rocks do not show any clear covariation. As Nd isotopic compositions are not fractionated by sedimentary processes, the scatter in Figure 7 may reflect disturbance of Sr isotopic compositions during erosion, weathering, transport and diagenesis of the sediments. Studies of the geochemistry of present-day Suspended Particulate Matter (SPM) transported by South American Equatorial rivers have pointed out the much higher variability of Sr isotopic composition of SPM when compared with corresponding Nd isotopic composition over a 1 year hydrological cycle (Viers et al., 2008). This study also highlights that the Nd isotopic composition of SPM is a much more robust provenance tracer than the Sr isotopic composition.

5.2. Provenance of Cretaceous Sediments in the Eastern Central Atlantic Ocean

Based on $\epsilon_{Nd(0)}$ variation, we can propose a three-step evolution for the paleogeographic evolution of the WAC (Figure 8).

5.2.1. Albian-Middle Cenomanian

Overall, the Albian-Middle Cenomanian DSDP samples yield the highest $\epsilon_{Nd(0)}$ values and the largest range of variation (−5.5 to −15) when compared with other Cretaceous DSDP samples (Figure 8a). This spatial heterogeneity implies distinct provenances and hence the coexistence of several small drainage basins restricted to peripheral domains of the WAC. The lowest $\epsilon_{Nd(0)}$ values (−14.9 and −15) correspond to samples from DSDP site 369 situated off the Mauritanian margin. These values are similar to those of modern detritus deposited in the Atlantic Ocean (Grousset et al., 1998; Meyer et al., 2011) and the Late Cretaceous-

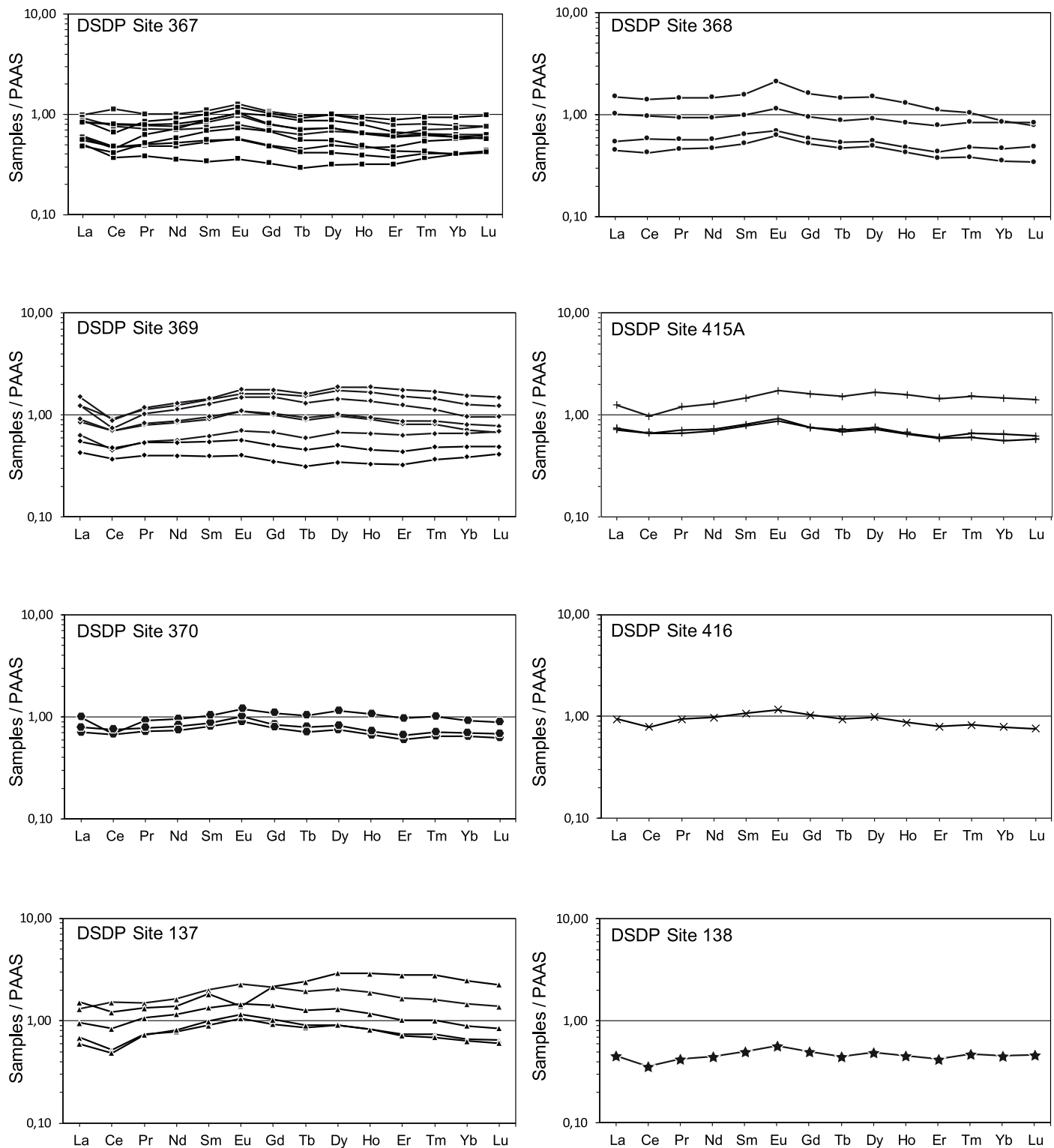


Figure 5. Rare earth element (REE) contents normalized to PAAS (Taylor & McLennan, 1985) for DSDP sites 367, 368, 369, 370, 137, 415A, and 416.

Early Eocene sedimentary rocks of the Tarfaya Basin in South-West Morocco (Ali et al., 2014). In comparison to present-day African catchment areas, such $\varepsilon_{\text{Nd}(0)}$ values are similar to the clays from the Congo River supplied predominantly by Precambrian terrains (Bayon et al., 2015). This suggests an unradiogenic Precambrian source as the main source of terrigenous sediments to the area of DSDP site 369. The Proterozoic

Table 3
Nd-Sr Isotopic Systematics of Sedimentary Rocks Analyzed in This Study

Leg-site-core	Top depth (mbsf)	Age	Sr (ppm)	$^{87}\text{Sr}/^{86}\text{Sr}$	$\pm 2\sigma$	Nd (ppm)	$^{143}\text{Nd}/^{144}\text{Nd}$	$\pm 2\sigma$	$\epsilon_{\text{Nd}(0)}$	$\pm 2\sigma$
14-137-6	218.31	Turonian- Campanian	59.8	0.727554	0.000011	52.1	0.512243	0.000026	-7.7	0.5
14-137-8	267.18	Late Cenomanian	28.6	0.730165	0.000011	25.2	0.512124	0.000013	-10.0	0.3
14-137-13	321.63	Early Cenomanian	44.1	0.722495	0.000010	26.2	0.512188	0.000021	-8.8	0.4
14-137-14	343.32	Early Cenomanian	17.1	0.717951	0.000015	44.1	0.512663	0.000015	0.5	0.3
14-137-16	376.98	Late Albian	34.4	0.729592	0.000028	37.2	0.512149	0.000018	-9.5	0.4
14-138-6	428.08	Cenomanian	20.8	0.737880	0.000010	14.3	0.512065	0.000014	-11.2	0.3
41-367-15	475.55	Late Cretaceous-Paleogene (Campanian-Maastrichtian?)	115.9	0.715854	0.000009	32.2	0.511905	0.000027	-14.3	0.5
41-367-16	542.04	No older than Turonian	139.0	0.716095	0.000009	24.5	0.511900	0.000018	-14.4	0.4
41-367-17	621.54	No older than Turonian	165.7	0.713189	0.000010	22.4	0.512031	0.000017	-11.8	0.3
41-367-18	638.02	Late Cenomanian-Early Turonian	133.0	0.714679	0.000009	11.4	0.512002	0.000018	-12.4	0.4
41-367-19	646.53	Late to Middle Cenomanian	143.7	0.713916	0.000011	15.4	0.512028	0.000021	-11.9	0.4
41-367-23	779.54	Albian	118.2	0.710894	0.000009	25.8	0.512241	0.000026	-7.7	0.5
41-367-26	915.72	Early Aptian to Hauterivian	90.0	0.732661	0.000016	23.2	0.512097	0.000015	-10.6	0.3
41-367-27	940.28	Early Aptian to Hauterivian	64.9	0.726645	0.000013	16.6	0.512011	0.000021	-12.2	0.4
41-367-31	1,053.33	Early Valanginian to Berriasian	38.1	0.740286	0.000012	18.7	0.512089	0.000015	-10.7	0.3
41-368-53	755.25	Late Cretaceous (und., no older than Campanian?)	61.6	0.724783	0.000053	18.4	0.511865	0.000014	-15.1	0.3
41-368-55-2	839.57	Late Cretaceous (und., Campanian?)	69.8	0.718791	0.000014	47.3	0.511961	0.000012	-13.2	0.2
41-368-56	847.06	Late Cretaceous (und., younger than Turonian)	35.7	0.715137	0.000011	15.1	0.511925	0.000017	-13.9	0.3
41-368-57	896.09	Late Cretaceous (und., younger than Turonian)	122.6	0.715087	0.000013	30.0	0.512047	0.000016	-11.5	0.3
41-369-A38	397.02	Campanian-Maastrichtian	76.6	0.717501	0.000009	27.3	0.511892	0.000015	-14.6	0.3
41-369-38F	397.02	Campanian-Maastrichtian	150.9	0.712316	0.000010	28.2	0.511893	0.000014	-14.5	0.3
41-369-39	405.2	Campanian	146.4	0.721748	0.000013	39.8	0.511894	0.000015	-14.5	0.3
41-369-A40	415.99	Campanian	104.8	0.718565	0.000016	42.1	0.512120	0.000014	-10.1	0.3
369-41-1	423.14	Campanian	149.9	0.716708	0.000012	36.4	0.512038	0.000015	-11.7	0.3
41-369-41-3	426.45	Campanian	342.6	0.711424	0.000028	18.2	0.511906	0.000011	-14.3	0.2
41-369-43	443.16	Late Albian	72.2	0.728915	0.000010	12.7	0.511873	0.000032	-14.9	0.6
41-369-47	481.08	Early Albian	69.0	0.730963	0.000012	17.3	0.511870	0.000014	-15.0	0.3
41-370-20	674.27	Late Albian-Early Cenomanian	79.5	0.712865	0.000012	23.4	0.512354	0.000022	-5.5	0.4
41-370-22	694.08	Late Albian-Early Cenomanian	113.6	0.710413	0.000010	25.9	0.512297	0.000046	-6.7	0.9
41-370-27	753.03	Albian	83.2	0.726263	0.000015	30.7	0.512062	0.000017	-11.2	0.3
50-415-7	509.69	Cenomanian-Coniacian	161.4	0.710719	0.000018	41.1	0.512008	0.000023	-12.3	0.4
50-415-9	645.22	Middle Cenomanian	75.7	0.711342	0.000014	23.3	0.512269	0.000041	-7.2	0.8
50-415-13	957.34	Early Cenomanian	57.7	0.715963	0.000017	22.3	0.512176	0.000037	-9.0	0.7
50-416-6	891.25	Late Aptian-Early Albian	93.3	0.727969	0.000010	31.3	0.511996	0.000017	-12.5	0.3
CM1-9		Santonian-Early Campanian (probable)		0.719789	0.000006		0.512142	0.000042	-9.7	0.8
CM1-7		Late Cenomanian-Early Turonian		0.722352	0.000007		0.512456	0.000018	-3.6	0.4
CM1-6		Late Cenomanian-Early Turonian		0.722165	0.000005		0.512377	0.000050	-5.1	1.0
CM1-5		Late Cenomanian-Early Turonian		0.714847	0.000005		0.512067	0.000048	-11.1	0.9
CM1-4		Late to Middle Cenomanian		0.715985	0.000005		0.512111	0.000020	-10.3	0.4
CM1-3		Early Cenomanian to Middle/Late Cenomanian		0.714537	0.000009		0.512031	0.000016	-11.8	0.3
CM1-2		Middle Albian		0.734570	0.000007		0.512063	0.000056	-11.2	1.1
CM1-1		Early Aptian		0.719619	0.000005		0.511970	0.000010	-13.0	0.2

Note. 2σ is the internal analytical error.

domains of the eastern Reguibat Shield seem the best candidates for this clastic supply since they have $\epsilon_{\text{Nd}(0)}$ values that are closely similar to the DSDP site samples (Peucat et al., 2005).

In the northern WAC domains, the $\epsilon_{\text{Nd}(0)}$ values are more radiogenic and increase from -11.2 to -5.5 at DSDP site 370 and from -9 to -7.2 at DSDP site 415A, suggesting a regional change in the provenance (Figure 8a). The Albian $\epsilon_{\text{Nd}(0)}$ values of -11.2 (DSDP site 370) and -12.5 (DSDP site 416) and the Eu anomalies ($\text{Eu}/\text{Eu}^* \sim 0.71$ -0.73) are similar to those measured in modern clays from the "Niger sub delta" ($\epsilon_{\text{Nd}(0)} = -11.9$ and $\text{Eu}/\text{Eu}^* \sim 0.71$; Bayon et al., 2015). As the Niger River catchment drains both Paleozoic and Precambrian terrains (Milesi et al., 2010), we suggest that Albian sedimentation at the DSDP site 370 was initially supplied by a mixed Paleozoic/Precambrian source. The lack of a significant change in Eu anomalies, or in Cr/Th and Th/Sc ratios, implies that the rise in $\epsilon_{\text{Nd}(0)}$ is not caused by an increasing supply of

more mafic detrital material from the same mixed Paleozoic/Precambrian source, but is rather linked to enhanced inputs from younger crustal sources. This could be related to a greater contribution from Hercynian and older Paleozoic rocks of the Meseta, Anti-Atlas and High Atlas Mountains, which show an average $\varepsilon_{\text{Nd}(0)}$ value of -5.6 (Figure 8a and supporting information Table S1).

The shallow-marine samples of CM1 well yield $\varepsilon_{\text{Nd}(0)}$ values intermediate between modern Nile River clays ($\varepsilon_{\text{Nd}(0)} = -7.1$; Bayon et al., 2015) and modern Niger River clays ($\varepsilon_{\text{Nd}(0)} = -11.9$; Bayon et al., 2015), which are derived from the erosion of Paleozoic/Hercynian units and mixed Paleozoic/Precambrian domains, respectively (Bayon et al., 2015; Milesi et al., 2010). This suggests that the sediments in CM1 well were supplied by a drainage system eroding both Paleozoic and Precambrian rocks. On the one hand, the Precambrian sources may be located in the northwestern part of the Leo-Man domain (Figure 8a). On the other hand, erosion of the Paleozoic sedimentary rocks of the Bowe Basin, as well as the Hercynian massifs of the Mauritanides could supply Paleozoic/Hercynian terrigenous detritus to the CM1 site, since these domains are considered to have been emerged from the Albian to the Cenomanian (Guiraud et al., 2005; Figure 8a).

The deepwater DSDP samples from Sites 137 and 367 have $\varepsilon_{\text{Nd}(0)}$ values higher than those from the shallow-marine CM1 well, suggesting that sediments from the latter were not supplied by the same drainage basin. These less negative $\varepsilon_{\text{Nd}(0)}$ values suggest an increased input of younger detritus to these deepwater sediments compared with the shallow-marine CM1 well. We exclude a South American provenance

because Cretaceous sediments deposited on the South American margin have much lower $\varepsilon_{\text{Nd}(0)}$ values (-15.2 to -16.2 ; Martin et al., 2012). A North American provenance can also be excluded because the samples from DSDP sites 138 and 137 do not have the same isotopic signature. As the samples from deepwater DSDP sites 137 and 367 have $\varepsilon_{\text{Nd}(0)}$ values close to the DSDP site 415 samples, this rather suggests a similar provenance. This implies the influence of oceanic currents transporting detritus from the Moroccan Atlantic coast to the central part of the Equatorial Atlantic Ocean, while preventing the arrival of material from the Senegalese continental shelf (CM1). This scenario agrees very well with the southwestward oceanic dispersion of palygorskite clay minerals from Morocco (Pletsch et al., 1996).

5.2.2. Late Cenomanian-Turonian

Compared with data for the previous interval, the $\varepsilon_{\text{Nd}(0)}$ values drop by -4.1 to -4.7 units for DSDP site 367 and by -5.1 units for DSDP site 415A (Figure 8b). This contrasts with drops of -0.8 to -1.5 units recorded at DSDP site 137 and -0.8 to -1.8 units on the Demerara Rise (Martin et al., 2012, Figure 8b). A positive $\varepsilon_{\text{Nd}(0)}$ excursion of $+8.3$ units is observed in the Late Cenomanian-Turonian sediments from the CM1 well. Owing to the Late Cenomanian and Turonian hiatus at DSDP sites 370, 416, and 369, this interval is only sparsely represented in Morocco (Figure 8b). Nevertheless, one sample from DSDP site 415A displays a low $\varepsilon_{\text{Nd}(0)}$ value of -12.3 which is in the same range as recorded at DSDP sites 367 and 368. This suggests that a long-term decrease of $\varepsilon_{\text{Nd}(0)}$ values also occurred in the northern part of the WAC. When compared to the catchments of modern African rivers, the lack of significant differences in $\varepsilon_{\text{Nd}(0)}$ values between the sedimentary rocks from DSDP sites 415A, 137, and 367 and modern Niger River sediments suggests the existence of mixed Paleozoic/Precambrian sources. When compared with older sedimentary rocks, the shift toward more negative $\varepsilon_{\text{Nd}(0)}$ values argues for increasing inputs of Precambrian detrital material to the eastern Central Atlantic Basin during the Late Cenomanian-Turonian. The reduced contribution of Paleozoic sources and increasing contribution of Precambrian sources may result from an extension of drainage areas toward the cratonic basement of the Reguibat and Leo-Man shield areas. This is because

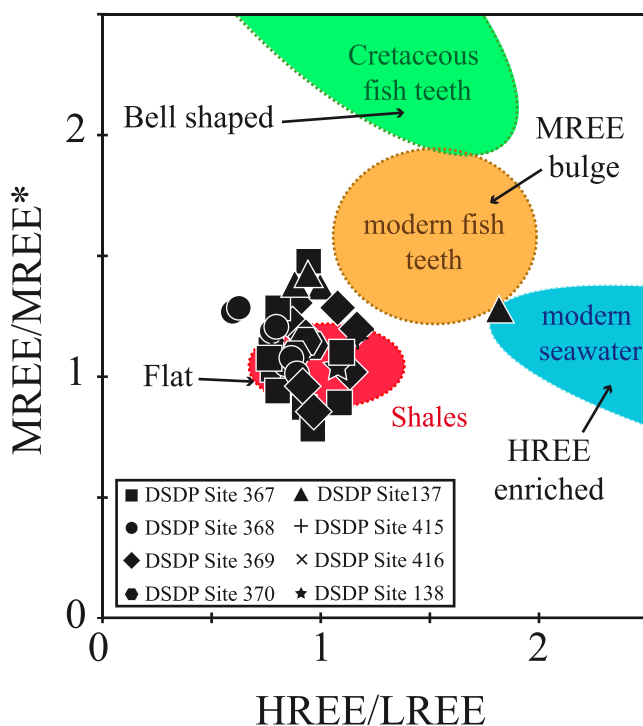


Figure 6. HREE/LREE versus MREE/MREE* diagram. HREE/LREE and MREE/MREE* values are calculated following Martin et al. (2010) where $\text{HREE} = \text{Tm} + \text{Yb} + \text{Lu}$, $\text{LREE} = \text{La} + \text{Pr} + \text{Nd}$, $\text{MREE} = \text{Gd} + \text{Tb} + \text{Dy}$ (all PAAS normalized), and $\text{MREE}^* = \text{the average of HREE} + \text{LREE}$. The MREE bulge and “bell-shaped” REE profiles correspond to REE patterns observed in fish teeth, Fe-Mn oxides, organic matter and pore waters, while “HREE-enriched” profiles correspond to modern sea water (Huck et al., 2016; Moiroud et al., 2016). These end-members reflect the REE contents of marine sediments influenced by seawater or authigenic phases, while “flat” REE patterns are characteristic of continental clays (see Huck et al., 2016; Moiroud et al., 2016 for a review). Samples from each DSDP site are represented by specific symbols used in Figures 4 and 5. Only one sample (sample 14–137–14) plot in the seawater field, and is therefore considered as strongly affected by marine authigenesis (see text for explanation).

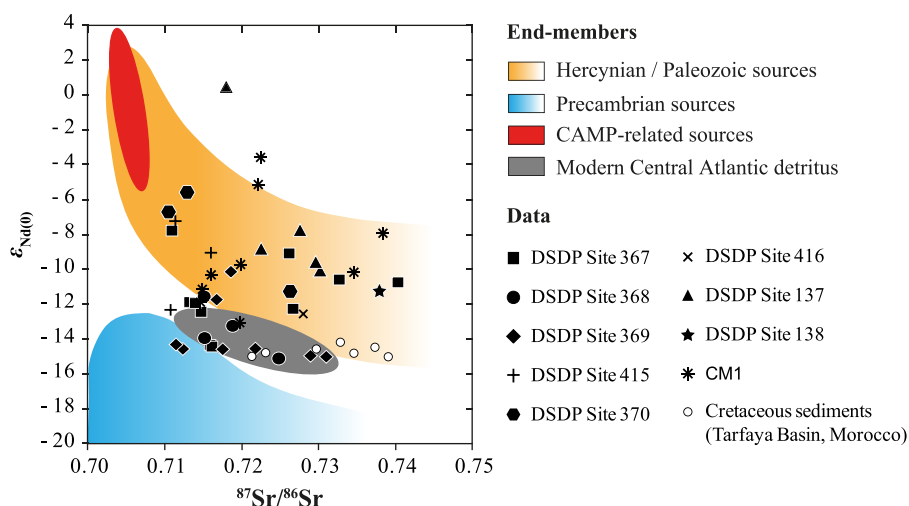


Figure 7. Cross plots of $\epsilon_{\text{Nd}(0)}$ and $^{87}\text{Sr}/^{86}\text{Sr}$ values for well CM1 and DSDP sites 367, 368, 369, 370, 137, 415A, and 416. The isotopic fields of potential end-members are based on a compilation of published data (see supporting information Table S1). Values for Cretaceous sediments in the Tarfaya Basin are taken from Ali et al. (2014). The positive $\epsilon_{\text{Nd}(0)}$ value of the Early Cenomanian sample of DSDP 137 (sample 14–137-14) is interpreted to reflect Nd input from the mid oceanic ridge (see text for explanation).

most Paleozoic source areas such as the Meseta (Morocco) or the Bowe Basin were flooded during this time interval (Guiraud et al., 2005, Figure 8b). However, this long-term decrease in $\epsilon_{\text{Nd}(0)}$ values is not recorded by samples from the shallow-marine CM1 well, which show a positive excursion of +8.5 to +6 epsilon units. This suggests a greater local contribution from younger Paleozoic/Hercynian terrains probably corresponding to the Mauritanides (Figure 8b). Moreover, the discrepancy between the $\epsilon_{\text{Nd}(0)}$ values from CM1 well and DSDP site 367 indicate that sediments at this deepwater site were still not sourced by clastic supply from the Mauritanides.

5.2.3. Campanian-Maastrichtian

Compared with the $\epsilon_{\text{Nd}(0)}$ values for the previous time interval, the $\epsilon_{\text{Nd}(0)}$ values of the Campanian-Maastrichtian sedimentary rocks are marked by a negative shift of -1.9 to -4 units (Figure 8c). A decrease of -6 units is also recorded in the CM1 sample on the platform, as well as in the Campanian-Maastrichtian sedimentary rocks of the Demerara Rise showing changes by -0.6 and -2.6 units toward less radiogenic Neodymium isotopic composition (Martin et al., 2012). The $\epsilon_{\text{Nd}(0)}$ values of Campanian-Maastrichtian DSDP sedimentary rocks are close to the Precambrian end-member (Figure 7) and similar to values observed in present-day marine sediments off the Northwest African Margin (Grousset et al., 1998; Meyer et al., 2011) and modern sediments deposited by the Congo River (Bayon et al., 2015). As present-day sediments are supplied by Precambrian sources, this suggests that Precambrian terrains represent the predominant source of clastic supply along the Western African Margin during the Campanian-Maastrichtian.

The Campanian-Maastrichtian sedimentary rocks of DSDP site 137 show an opposite trend with a positive shift of +2.6 units ($\epsilon_{\text{Nd}(0)} \sim -7.7$, Figure 8c). This could reflect an increasing contribution of volcanic sediments/rocks from the mid-ocean ridge. However, the REE pattern of this sample is flat with respect to PAAS and we find no difference in Eu anomaly compared with the other analyzed samples (Table 2). Hence, we can rule out a significant contribution from volcanic sources. The potential source area for this sedimentary rock could lie farther to the North, since the $\epsilon_{\text{Nd}(0)}$ value of -7.7 is within the range of Paleozoic sediments from the Meseta, Anti-Atlas and High Atlas Mountains, as well as NW Tethyan sediments (i.e., -12 to -6 ϵ_{Nd} units; Dera et al., 2015) or North American Appalachian rocks (-10 to -5 ϵ_{Nd} units, Patchett et al., 1999).

5.3. Possible Mechanisms for Drainage Reorganization

Our results indicate that the Albian-Middle Cenomanian interval is characterized by at least three main paleodrainage basins with restricted extensions toward the hinterland: two of them draining Paleozoic/Hercynian units in the northern and central parts of the WAC and another draining Precambrian units in the Reguibat Shield region (Figure 8a). This drainage partitioning implies that catchment basins could have

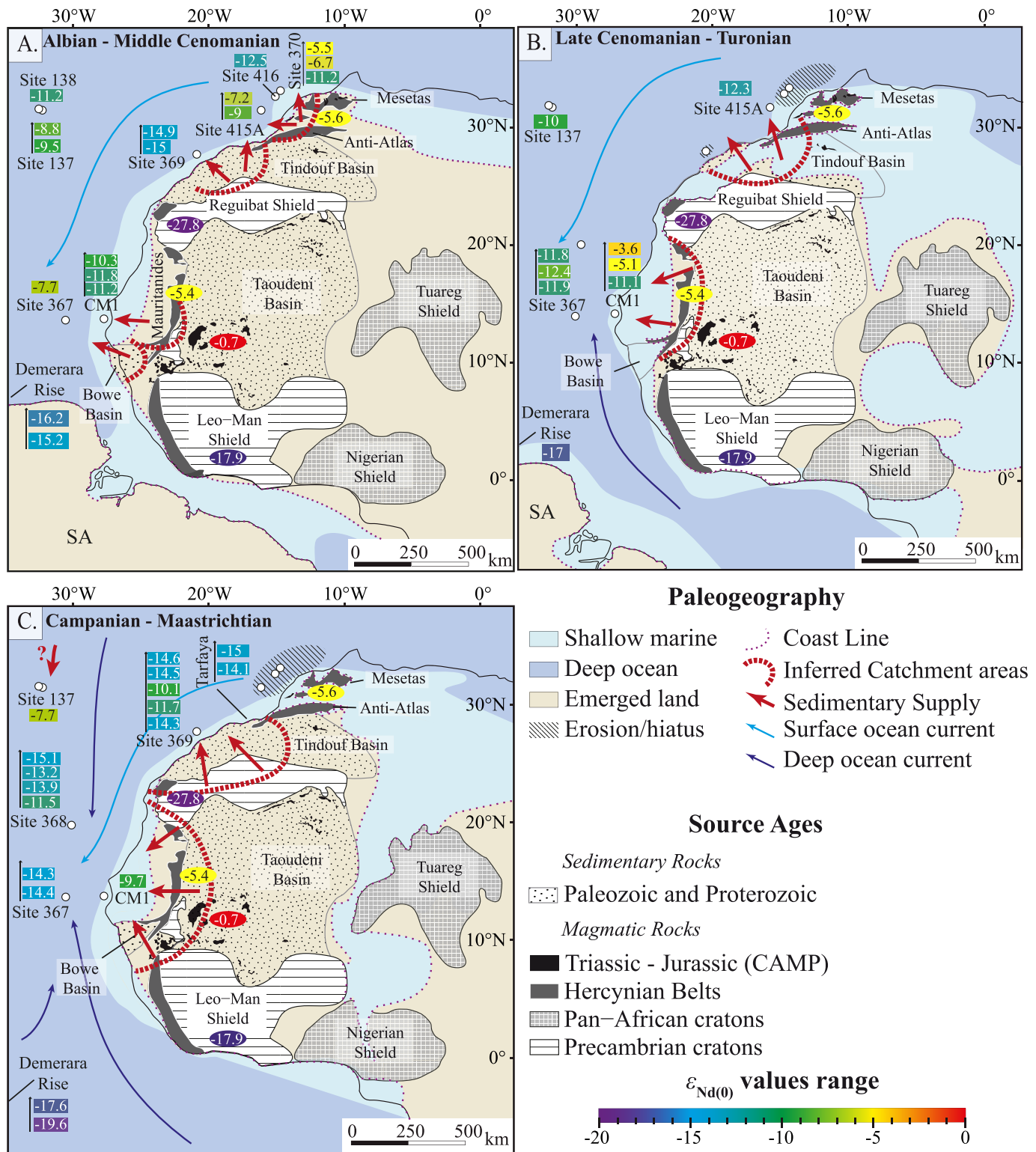


Figure 8. Paleogeographic maps (modified from Guiraud et al., 2005; Scotese & Golonka, 1997) showing the $\epsilon_{Nd(0)}$ values of sediments along the Northwestern African Margin for three periods: (a) from the Albian to the Middle Cenomanian; (b) from the Late Cenomanian to the Turonian; (c) from the Campanian to the Maastrichtian. The $\epsilon_{Nd(0)}$ values for samples at each site are represented in stratigraphic order. The $\epsilon_{Nd(0)}$ data from the Demerara Rise and Tarfaya Basin are from Martin et al. (2012) and Ali et al. (2014), respectively. The color-coded scale indicates ϵ_{Nd} values ranging from radiogenic in red to highly unradiogenic values. The average $\epsilon_{Nd(0)}$ value of each potential source is illustrated by colored ellipses. Source ages are simplified from Milesi et al. (2010). SA, South America. Surface and deep oceanic current are taken from Puc  at et al. (2005) and Robinson & Vance (2012).

been separated by areas of relief on the periphery of the WAC. The existence of topographic highs acting as natural barriers dividing and limiting the extension of drainage areas suggests that significant uplift may have affected the WAC during the Albian-Middle Cenomanian. The mechanisms causing these uplifts may be related to the onset of opening of the South and Equatorial Atlantic Ocean during the Early Cretaceous and Late Albian (Flicoteaux et al., 1988; Förster, 1978; Moulin et al., 2010) or increasing compressive stress in northern, central, eastern and southern region of Africa induced by the anticlockwise rotation of Africa during this period (Guiraud & Bosworth, 1997; Guiraud & Maurin, 1991; Moulin et al., 2010) or a combination of all these factors.

During the Late Cenomanian-Turonian, with the exception of the Senegalese continental shelf (CM1 well, Figure 8b), there was an increased supply of Precambrian detritus to the deepwater basin (DSDP sites 367, 137, and 415A, Figure 8b). This change may be due to a reduced contribution of proximal Hercynian/Paleozoic units probably caused by paleogeographic and physiographic changes in the Mauritania-Senegal basin. These changes could be triggered by the cessation of the flexure of the western edge of the basin, resulting in the burial of its substratum and progressive flattening of the relief (Flicoteaux et al., 1988; Leprêtre et al., 2015). These events are coeval with crustal thinning occurring in the Mauritania-Senegal basin and in Guinea that could be related to the opening of the Equatorial Atlantic Ocean (Förster, 1978; Flicoteaux et al., 1988; Latil-Brun & Lucazeau, 1988). In addition, the Cenomanian-Turonian boundary records the Cretaceous maximum flooding which led to the expansion of shelf seas (Schlanger & Jenkyns, 1976) toward the Mauritania and the Reguibat Shield. Associated with a more flattened topography, this marine transgression may have flooded some of the Paleozoic and Hercynian proximal source areas (e.g., the Bowe Basin, Meseta, Guiraud et al., 2005; Figure 8b). This flooding may be responsible for paleogeographic changes in the Mauritania-Senegal basin and may have induced a reorganization of the drainage pathways. Indeed, Barnett-Moore et al., (2017) point out that the combined action of dynamic changes in topography and global sea-level fluctuations led to major incursions of the peripheral regions of Northwest Africa during this period. Thus, the maximum flooding of the Cenomanian-Turonian boundary, associated with changes in the paleotopography, could also partly explain the decrease in Paleozoic inputs when compared with the Albian-Middle Cenomanian.

The Campanian-Maastrichtian is characterized by increasing inputs of Precambrian detritus along the Northwest African Margin (except at DSDP site 137 and CM1, Figure 8c). This implies an expansion of drainage areas toward the east and the inner units of the WAC. As recorded by low-temperature thermochronology data (Leprêtre et al., 2015), the Late Cretaceous to Early Paleogene uplift of the Saharan region of South Morocco may have caused increasing erosion of Precambrian rocks of the Reguibat Shield, which could explain the lowering of the $\varepsilon_{Nd(0)}$ values along the northern margin of the WAC. This uplift has been related to the onset of Africa/Europe convergence (Leprêtre et al., 2015) and could be correlated with the "Santonian Compressional Event" (84–80 Ma; Binks & Fairhead, 1992; Guiraud & Bosworth, 1997). This event is related to the convergence between Europe and Africa (Olivet et al., 1984; Rosenbaum et al., 2002) as well as the change in poles of rotation for the opening of the Atlantic Ocean (Binks & Fairhead, 1992; Guiraud & Bosworth, 1997; Guiraud et al., 1992; Klitgord & Schouten, 1986). Indeed, it is responsible for the inversion of several sedimentary basins in Africa and the reactivation of some faults related to the Panafrican and Hercynian sutures in the WAC. Such an event may also have impacted the drainage pathways leading to the severe erosion of Precambrian units in the hinterland of the WAC (e.g., the Reguibat Shield, the Leo-Man Shield, and the Taoudeni Basin, Figure 8c).

5.4. Implications for Atlantic Ocean Paleocirculation

Finally, our results on provenance also have some implications regarding oceanic circulation in the Central Atlantic basin during the Cretaceous. During the Early Cretaceous, a slow to sluggish oceanic circulation with very little renewal of deepwater and a prominent water column stratification likely prevailed in the Atlantic Ocean (Barron, 1983; Bralower & Thierstein, 1984). Only water-depths shallower than 500 m off the western Gondwana margins might have been affected by surface currents from the north (Tethys Ocean; Poulsen et al., 2001; Pucéat et al., 2005). In contrast, paleogeographic changes linked to the incipient opening of the Equatorial Atlantic Ocean (90–94 Ma) would have progressively led to increasing oceanic circulation and better ventilation of the seafloor by bottom currents during the Late Cretaceous in the entire Central Atlantic Ocean (Donnadieu et al., 2016; Poulsen et al., 2001). This change might have resulted in the formation of deepwater currents that originated from the eastern Pacific and the South Atlantic Oceans,

and flowed northward to the Central Atlantic Ocean (Donnadieu et al., 2016; Poulsen et al., 2001; Robinson & Vance, 2012; Trabucho Alexandre et al., 2010; Voigt et al., 2013).

The difference in $\varepsilon_{\text{Nd}(0)}$ values between the shallow-marine CM1 samples and deepwater DSDP samples suggest that the deep oceanic basin of the Central Atlantic Ocean only rarely received clastic inputs from the Senegal-Mauritanides coast (i.e., the drainage basin that supplied the CM1 samples) during the Cretaceous. This indicates that shallow or deep boundary currents might have prevented any direct sedimentary input from the adjacent coast by scattering fine particles along the margin. This observation is in agreement with an increasing oceanic circulation and better ventilation of the seafloor by bottom currents for the Late Cretaceous period (Donnadieu et al., 2016). However, it contradicts the hypothesis of sluggish oceanic circulation in the Early Cretaceous because the disconnection between shallow and deep layers observed here prevailed as early as the Middle Aptian. Despite the fact that evidences for deep oceanic currents are lacking for the southern part of the Central Atlantic Ocean off Mauritania and Guinea, the presence of contourite drifts in Early Cretaceous deposits offshore Morocco suggests that a deep oceanic current may have existed in this area (Dunlap et al., 2013). However, more work is needed to better document the Early Cretaceous oceanic circulation in the southern part of the Central Atlantic Ocean.

6. Conclusion

Based on the major and trace element contents and Sr-Nd isotopic composition of sedimentary rocks sampled in the eastern Central Atlantic Ocean, this provenance study highlights a large-scale reorganization of drainage pathways in Northwest Africa during the Cretaceous. Three steps are identified, with major implications regarding the evolution of WAC drainage system:

1. The Albian-Middle Cenomanian is characterized by the presence of at least three restricted subdrainage basins with distinct provenances (Hercynian/Paleozoic, Precambrian, and mixed Precambrian/Paleozoic) and limited extension toward the inner parts of the craton.
2. The Late Cenomanian-Turonian DSDP sediments deposited in the deepwater domain have more homogeneous and more negative $\varepsilon_{\text{Nd}(0)}$ values interpreted as reflecting an increasing supply of clastic detritus from the inner parts of the Precambrian cratons.
3. The Campanian-Maastrichtian sediments deposited along the Northwest African Margin are characterized by a lowering of $\varepsilon_{\text{Nd}(0)}$ values by -3 to -4 units. This is interpreted as the record of a shift from a mixed Paleozoic/Precambrian source to a Precambrian source.

Acknowledgments

This study was funded by Total Exploration and Production through the R&D project "Sedimentology of organic matter in deep oceanic basins" and the Actions Marges project "Traçages des sources de la marge du nord ouest de l'Afrique" funded by INSU-CNRS, TOTAL, IFREMER, and BRGM. Jung-Hyun Kim was also partly supported by a grant from the National Research Foundation of Korea (NRF) funded by the Korea government (MSIP) (2016R1A2B3015388). This work used samples provided by the Deep Sea Drilling Project (DSDP), which is sponsored by the US National Science Foundation and participating countries under the management of the Joint Oceanographic Institutions (JOI), Inc. We thank the Editor Janne Blichert-Toft and three anonymous reviewers for helpful comments that helped us to greatly improve this manuscript. Michael Carpenter postedited the English style and grammar. The data used are listed in the tables, figures, and in supporting information (text and supporting information Tables S1–S3).

The changes in provenance and drainage proposed here correspond to major geodynamic events of the WAC linked to the opening of the South and Equatorial Atlantic Oceans, followed by convergence of the African-Eurasian tectonic plates. The differences in $\varepsilon_{\text{Nd}(0)}$ values between shallow-marine CM1 samples and deepwater DSDP sites throughout the Cretaceous suggests that the deepwater sediments of the Central Atlantic Ocean were not derived from the Mauritanian margin. This suggests the existence of an ocean current capable of preventing the arrival of these sediments during the Cretaceous.

References

- Ajaji, T., Weis, D., Giret, A., & Bouabdellah, M. (1998). Coeval potassic and sodic calc-alkaline series in the post-collisional Hercynian Tann-cherfi intrusive complex, northeastern Morocco: Geochemical, isotopic and geochronological evidence. *Lithos*, 45(1–4), 371–393. [https://doi.org/10.1016/S0024-4937\(98\)00040-1](https://doi.org/10.1016/S0024-4937(98)00040-1)
- Ali, S., Stattegger, K., Garbe-Schönberg, D., Frank, M., Kraft, S., & Kuhnt, W. (2014). The provenance of Cretaceous to Quaternary sediments in the Tarfaya basin, SW Morocco: Evidence from trace element geochemistry and radiogenic Nd–Sr isotopes. *Journal of African Earth Sciences*, 90, 64–76. <https://doi.org/10.1016/j.jafrearsci.2013.11.010>
- Allègre, C. J., Dupré, B., Lambret, B., & Richard, P. (1981). The subcontinental versus suboceanic debate, I Lead-neodymium-strontium isotopes in primary alkali basalts from a shield area the Ahaggar volcanic suite. *Earth and Planetary Science Letters*, 52(1), 85–92. [https://doi.org/10.1016/0012-821X\(81\)90210-7](https://doi.org/10.1016/0012-821X(81)90210-7)
- Asiedu, D. K., Hegner, E., Rocholl, A., & Atta-Peters, D. (2005). Provenance of late Ordovician to early Cretaceous sedimentary rocks from southern Ghana, as inferred from Nd isotopes and trace elements. *Journal of African Earth Sciences*, 41(4), 316–328. <https://doi.org/10.1016/j.jafrearsci.2005.05.003>
- Azzouni-Sekkal, A., Liégeois, J. P., Bechiri-Benmerzoug, F., Belaidi-Zinet, S., & Bonin, B. (2003). The "Taourirt" magmatic province, a marker of the closing stage of the Pan-African orogeny in the Tuareg Shield: Review of available data and Sr–Nd isotope evidence. *Journal of African Earth Sciences*, 37(3–4), 331–350. <https://doi.org/10.1016/j.jafrearsci.2003.07.001>
- Barnett-Moore, N., Hassan, R., Müller, R. D., Williams, S. E., & Flament, N. (2017). Dynamic topography and eustasy controlled the paleogeographic evolution of northern Africa since the mid-Cretaceous. *Tectonics*, 36, 929–944. <https://doi.org/10.1002/2016TC004280>

- Barron, E. J. (1983). A warm, equable Cretaceous: The nature of the problem. *Earth-Science Reviews*, 19(4), 305–338.
- Bayon, G., German, C. R., Boella, R. M., Milton, J. A., Taylor, R. N., & Nesbitt, R. W. (2002). An improved method for extracting marine sediment fractions and its application to Sr and Nd isotopic analysis. *Chemical Geology*, 187(3–4), 179–199. [https://doi.org/10.1016/S0009-2541\(01\)00416-8](https://doi.org/10.1016/S0009-2541(01)00416-8)
- Bayon, G., Toucanne, S., Skonieczny, C., André, L., Bermell, S., Cheron, S., et al. (2015). Rare earth elements and neodymium isotopes in world river sediments revisited. *Geochimica et Cosmochimica Acta*, 170, 17–38. <https://doi.org/10.1016/j.gca.2015.08.001>
- Bea, F., Montero, P., Haissen, F., & El Archi, A. (2013). 2.46 Ga kalsilite and nepheline syenites from the Awsard pluton, Reguibat Rise of the West African Craton, Morocco. Generation of extremely K-rich magmas at the Archean–Proterozoic transition. *Precambrian Research*, 224, 242–254. <https://doi.org/10.1016/j.precamres.2012.09.024>
- Bea, F., Montero, P., Haissen, F., Molina, J. F., Michard, A., Lazaro, C., et al. (2015). First evidence for Cambrian rift-related magmatism in the West African Craton margin: The Derraman Peralkaline Felsic Complex. *Gondwana Research*, 36, 423–438. <https://doi.org/10.1016/j.gr.2015.07.017>
- Binks, R. M., & Fairhead, J. D. (1992). A plate tectonic setting for Mesozoic rifts of West and Central Africa. *Tectonophysics*, 213(1–2), 141–151. [https://doi.org/10.1016/0040-1951\(92\)90255-5](https://doi.org/10.1016/0040-1951(92)90255-5)
- Blanc, A., Bernard-Griffiths, J., Caby, R., Caruba, C., Caruba, R., Dars, R., et al. (1992). U-Pb dating and isotopic signature of the alkaline ring complexes of Bou Naga (Mauritania): Its bearing on late Proterozoic plate tectonics around the West African Craton. *Journal of African Earth Sciences*, 14(3), 301–311. [https://doi.org/10.1016/0899-5362\(92\)90034-A](https://doi.org/10.1016/0899-5362(92)90034-A)
- Bodin, S., Meissner, P., Janssen, N. M., Steuber, T., & Mutterlose, J. (2015). Large igneous provinces and organic carbon burial: Controls on global temperature and continental weathering during the Early Cretaceous. *Global and Planetary Change*, 133, 238–253. <https://doi.org/10.1016/j.gloplacha.2015.09.001>
- Boher, M., Abouchami, W., Michard, A., Albarede, F., & Arndt, N. T. (1992). Crustal growth in West Africa at 2.1 Ga. *Journal of Geophysical Research*, 97(B1), 345–369. <https://doi.org/10.1029/91JB01640>
- Bouchez, J., Gaillardet, J., France-Lanord, C., Maurice, L., & Dutra-Maia, P. (2011). Grain size control of river suspended sediment geochemistry: Clues from Amazon River depth profiles. *Geochemistry, Geophysics, Geosystems*, 12, Q03008. <https://doi.org/10.1029/2010GC003380>
- Bralower, T. J., & Thierstein, H. R. (1984). Low productivity and slow deep-water circulation in mid-Cretaceous oceans. *Geology*, 12(10), 614–618.
- Burke, K., Dewey, J. F., & Kidd, W. S. F. (1976). Precambrian palaeomagnetic results compatible with contemporary operation of the Wilson cycle. *Tectonophysics*, 33(3–4), 287–299. [https://doi.org/10.1016/0040-1951\(76\)90149-9](https://doi.org/10.1016/0040-1951(76)90149-9)
- Carignan, J., Hild, P., Mevelle, G., Morel, J., & Yeghicheyan, D. (2001). Routine analyses of trace elements in geological samples using flow injection and low pressure on-line liquid chromatography coupled to ICP-MS: A study of geochemical reference materials BR, DR-N, UB-N, AN-G and GH. *Geostandards Newsletter*, 25(2–3), 187–198. <https://doi.org/10.1111/j.1751-908X.2001.tb00595.x>
- Cepek, P. (1978). *Mesozoic calcareous nannoplankton of the eastern North Atlantic, Leg 41* (Initial Reports of the Deep Sea Drilling Project 41, pp. 667–687). <https://doi.org/10.2973/dsdp.proc.41.114.1978>
- Clift, P. D., & Blusztajn, J. (2005). Reorganization of the western Himalayan river system after five million years ago. *Nature*, 438(7070), 1001–1003. <https://doi.org/10.1038/nature04379>
- Condie, K. C. (1993). Chemical composition and evolution of the upper continental crust: Contrasting results from surface samples and shales. *Chemical Geology*, 104(1–4), 1–37. [https://doi.org/10.1016/0009-2541\(93\)90140-E](https://doi.org/10.1016/0009-2541(93)90140-E)
- Cool, T., Katz, B., Dignes, T., Reimers, D., & Fleisher, R. (2008). Hydrocarbon source rock assessment and revised biostratigraphy of DSDP Site 369A, offshore Northwest African Margin. *Journal of Petroleum Geology*, 31(2), 117–133. <https://doi.org/10.1111/j.1747-5457.2008.00411.x>
- Cullers, R. L. (2000). The geochemistry of shales, siltstones and sandstones of Pennsylvanian–Permian age, Colorado, USA: Implications for provenance and metamorphic studies. *Lithos*, 51(3), 181–203. [https://doi.org/10.1016/S0016-7037\(99\)00063-8](https://doi.org/10.1016/S0016-7037(99)00063-8)
- Davison, I. (2005). Central Atlantic margin basins of North West Africa: Geology and hydrocarbon potential (Morocco to Guinea). *Journal of African Earth Sciences*, 43(1–3), 254–274. <https://doi.org/10.1016/j.jafrearsci.2005.07.018>
- De Baar, H. J. W., Bacon, M. P., Brewer, P. G., & Bruland, K. W. (1985). Rare earth elements in the Pacific and Atlantic Oceans. *Geochimica et Cosmochimica Acta*, 49(9), 1943–1959. [https://doi.org/10.1016/0016-7037\(85\)90089-4](https://doi.org/10.1016/0016-7037(85)90089-4)
- Deckart, K., Bertrand, H., & Liégeois, J.-P. (2005). Geochemistry and Sr, Nd, Pb isotopic composition of the Central Atlantic Magmatic Province (CAMP) in Guyana and Guinea. *Lithos*, 82, 289–314. <https://doi.org/10.1016/j.lithos.2004.09.023>
- Dera, G., Prunier, J., Smith, P. L., Haggart, J. W., Popov, E., Guzhov, A., et al. (2015). Nd isotope constraints on ocean circulation, paleoclimate, and continental drainage during the Jurassic breakup of Pangea. *Gondwana Research*, 27(4), 1599–1615. <https://doi.org/10.1016/j.gr.2014.02.006>
- Dewey, J. F., & Burke, K. (1974). Hot spots and continental break-up: Implications for collisional orogeny. *Geology*, 2(2), 57–60. [https://doi.org/10.1130/0091-7613\(1974\)2<57:HSACBI>2.0.CO;2](https://doi.org/10.1130/0091-7613(1974)2<57:HSACBI>2.0.CO;2)
- Dewey, J. F., Hempton, M. R., Kidd, W. S. F., Saroglu, F., & Şengör, A. M. C. (1986). Shortening of continental lithosphere: The neotectonics of Eastern Anatolia—A young collision zone. *Geological Society, Special Publications*, 19(1), 1–36. <https://doi.org/10.1144/GSL.SP.1986.019.01.01>
- Dia, A., Van Schmus, W. R., & Kröner, A. (1997). Isotopic constraints on the age and formation of a Palaeoproterozoic volcanic arc complex in the Kedougou Inlier, eastern Senegal, West Africa. *Journal of African Earth Sciences*, 24(3), 197–213. [https://doi.org/10.1016/S0899-5362\(97\)00038-9](https://doi.org/10.1016/S0899-5362(97)00038-9)
- D'Lemos, R. S., Inglis, J. D., & Samson, S. D. (2006). A newly discovered orogenic event in Morocco: Neoproterozoic ages for supposed Eburnean basement of the Bou Azzer inlier, Anti-Atlas Mountains. *Precambrian Research*, 147(1–2), 65–78. <https://doi.org/10.1016/j.precamres.2006.02.003>
- Donnadieu, Y., Pucéat, E., Moiroud, M., Guillocheau, F., & Deconinck, J. F. (2016). A better-ventilated ocean triggered by Late Cretaceous changes in continental configuration. *Nature Communications*, 7, 10316. <https://doi.org/10.1038/ncomms10316>
- Drake, E. T. (1976). Alfred Wegener's reconstruction of Pangea. *Geology*, 4(1), 41–44. [https://doi.org/10.1130/0091-7613\(1976\)4<41:AWROP>2.0.CO;2](https://doi.org/10.1130/0091-7613(1976)4<41:AWROP>2.0.CO;2)
- Dunlap, D., Wood, L., & Moscardelli, L. (2013). Seismic geomorphology of early North Atlantic sediment waves, offshore northwest Africa. *Interpretation*, 1(1), SA75–SA91. <https://doi.org/10.1190/INT-2013-0040.1>
- Dupuy, C., Marsh, J., Dostal, J., Michard, A., & Testa, S. (1988). Asthenospheric and lithospheric sources for Mesozoic dolerites from Liberia (Africa): Trace element and isotopic evidence. *Earth and Planetary Science Letters*, 87(1–2), 100–110. [https://doi.org/10.1016/0012-821X\(88\)90067-2](https://doi.org/10.1016/0012-821X(88)90067-2)
- El Baghdadi, M., El Boukhari, A., Jouider, A., Benyoucef, A., & Nadem, S. (2003). Calc-alkaline arc I-type granitoid associated with S-type granite in the Pan-African Belt of Eastern Anti-Atlas (Saghro and Ougnat, South Morocco). *Gondwana Research*, 6(4), 557–572. [https://doi.org/10.1016/S1342-937X\(05\)71007-8](https://doi.org/10.1016/S1342-937X(05)71007-8)

- Emery, K. O., & Uchupi, E. (1984). *The geology of the Atlantic Ocean*. Berlin, Germany: Springer Science & Business Media.
- Ennih, N., & Liégeois, J. P. (2008). The boundaries of the West African Craton, with special reference to the basement of the Moroccan metacratonic Anti-Atlas belt. *Geological Society, Special Publications*, 297(1), 1–17. <https://doi.org/10.1144/SP297.1>
- Errami, E., Bonin, B., Laduron, D., & Lasri, L. (2009). Petrology and geodynamic significance of the post-collisional Pan-African magmatism in the Eastern Saghro area (Anti-Atlas, Morocco). *Journal of African Earth Sciences*, 55(1–2), 105–124. <https://doi.org/10.1016/j.jafrearsci.2009.02.006>
- Essaifi, A., Samson, S., & Goodenough, K. (2014). Geochemical and Sr–Nd isotopic constraints on the petrogenesis and geodynamic significance of the Jebilet magmatism (Variscan Belt, Morocco). *Geological Magazine*, 151(4), 666–691. <https://doi.org/10.1017/S0016756813000654>
- Fedo, C. M., Nesbitt, H. W., & Young, G. M. (1995). Unraveling the effects of potassium metasomatism in sedimentary rocks and paleosols, with implications for paleoweathering conditions and provenance. *Geology*, 23(10), 921–924. [https://doi.org/10.1130/0091-7613\(1995\)023<0921:UTEOPM>2.3.CO;2](https://doi.org/10.1130/0091-7613(1995)023<0921:UTEOPM>2.3.CO;2)
- Fedo, C. M., Sircombe, K. N., & Rainbird, R. H. (2003). Detrital zircon analysis of the sedimentary record. *Reviews in Mineralogy and Geochemistry*, 53(1), 277–303. <https://doi.org/10.2113/0530277>
- Flicoteaux, R., Latil-Brun, M.-V., & Michaud, L. (1988). Histoire de la subsidence post-rift du bassin côtier mauritano-sénégal-guinéen. Relation avec l'amincissement crustal pendant la période jurassique à Crétacé inférieur. Comparaison avec l'évolution des marges péri-atlantiques au niveau de l'Atlantique Central et Equatorial (côte est des U.S.A., Sud-Sahara, Côte d'Ivoire et Plateau du Demerara). *Journal of African Earth Sciences*, 7(2), 345–359. [https://doi.org/10.1016/0899-5362\(88\)90079-6](https://doi.org/10.1016/0899-5362(88)90079-6)
- Foreman, H. P. (1978). *Mesozoic Radiolaria in the Atlantic Ocean off the Northwest Coast of Africa, Deep Sea Drilling Project, Leg 41* (Initial Reports of the Deep Sea Drilling Project). <https://doi.org/10.2973/dsdp.proc.41.117.1978>
- Förster, R. (1978). Evidence for an open seaway between northern and southern proto-Atlantic in Albian times. *Nature*, 272(5649), 158–159. <https://doi.org/10.1038/272158a0>
- Friedrich, O., Norris, R. D., & Erbacher, J. (2012). Evolution of middle to Late Cretaceous oceans—A 55 m.y. record of Earth's temperature and carbon cycle. *Geology*, 40(2), 107–110. <https://doi.org/10.1130/G32701.1>
- Fullgraf, T., Ndiaye, P. M., Blein, O., Buscail, F., Lahondère, D., Le Métour, J., et al. (2013). Silurian magmatism in eastern Senegal and its significance for the Paleozoic evolution of NW-Gondwana. *Journal of African Earth Sciences*, 78, 66–85. <https://doi.org/10.1016/j.jafrearsci.2012.08.003>
- Garzanti, E., Vezzoli, G., Andò, S., Lavé, J., Attal, M., France-Lanord, C., et al. (2007). Quantifying sand provenance and erosion (Marsyandi River, Nepal Himalaya). *Earth and Planetary Science Letters*, 258(3–4), 500–515. <https://doi.org/10.1016/j.epsl.2007.04.010>
- Gasquet, D., Barbey, P., Adou, M., & Paquette, J. L. (2003). Structure, Sr–Nd isotope geochemistry and zircon U–Pb geochronology of the granitoids of the Dabakala area (Côte d'Ivoire): Evidence for a 2.3 Ga crustal growth event in the Palaeoproterozoic of West Africa? *Precambrian Research*, 127(4), 329–354. [https://doi.org/10.1016/S0301-9268\(03\)00209-2](https://doi.org/10.1016/S0301-9268(03)00209-2)
- Gasquet, D., Leterrier, J., Mrini, Z., & Vidal, P. (1992). Petrogenesis of the Hercynian Tichka plutonic complex (Western High Atlas, Morocco): Trace element and Rb–Sr and Sm–Nd isotopic constraints. *Earth and Planetary Science Letters*, 108(1–3), 29–44. [https://doi.org/10.1016/0012-821X\(92\)90058-4](https://doi.org/10.1016/0012-821X(92)90058-4)
- Goldstein, S. L., O'Nions, R. K., & Hamilton, P. J. (1984). A Sm–Nd isotopic study of atmospheric dusts and particulates from major river systems. *Earth and Planetary Science Letters*, 70(2), 221–236. [https://doi.org/10.1016/0012-821X\(84\)90007-4](https://doi.org/10.1016/0012-821X(84)90007-4)
- Grousset, F. E., Parra, M., Bory, A., Martinez, P., Bertrand, P., Shimmield, G., et al. (1998). Saharan wind regimes traced by the Sr–Nd isotopic composition of subtropical Atlantic sediments: Last Glacial Maximum vs today. *Quaternary Science Reviews*, 17(4–5), 395–409. [https://doi.org/10.1016/S0277-3791\(97\)00048-6](https://doi.org/10.1016/S0277-3791(97)00048-6)
- Guiraud, R., Binks, R. M., Fairhead, J. D., & Wilson, M. (1992). Chronology and geodynamic setting of Cretaceous–Cenozoic rifting in West and Central Africa. *Tectonophysics*, 213(1–2), 227–234. [https://doi.org/10.1016/0040-1951\(92\)90260-D](https://doi.org/10.1016/0040-1951(92)90260-D)
- Guiraud, R., & Bosworth, W. (1997). Senonian basin inversion and rejuvenation of rifting in Africa and Arabia: Synthesis and implications to plate-scale tectonics. *Tectonophysics*, 282(1–4), 39–82. [https://doi.org/10.1016/S0040-1951\(97\)00212-6](https://doi.org/10.1016/S0040-1951(97)00212-6)
- Guiraud, R., Bosworth, W., Thierry, J., & Delplanque, A. (2005). Phanerozoic geological evolution of Northern and Central Africa: An overview. *Journal of African Earth Sciences*, 43(1–3), 83–143. <https://doi.org/10.1016/j.jafrearsci.2005.07.017>
- Guiraud, R., & Maurin, J. C. (1991). Le Rifting en Afrique au Cretace inferieur; synthese structurale, mise en evidence de deux etapes dans la genese des bassins, relations avec les ouvertures oceaniques peri-africaines. *Bulletin de la Société Géologique de France*, 162(5), 811–823. <https://doi.org/10.2113/gssgfbull.162.5.811>
- Hayes, D. E., Pimm, A. C., Benson, W. E., Berger, W. H., von Rad, U., Supko, P. R., et al. (1972). Site 137. *Deep Sea Drilling Project, Leg 14* (Initial Reports of the Deep Sea Drilling Project 14, pp. 85–134). <https://doi.org/10.2973/dsdp.proc.14.104.1972>
- Huck, C. E., van de Flierdt, T., Jiménez-Espejo, F. J., Bohaty, S. M., Röhl, U., & Hammond, S. J. (2016). Robustness of fossil fish teeth for seawater neodymium isotope reconstructions under variable redox conditions in an ancient shallow marine setting. *Geochemistry, Geophysics, Geosystems*, 17, 679–698. <https://doi.org/10.1002/2015GC006218>
- Jacobsen, S. B., & Wasserburg, G. J. (1980). Sm–Nd isotopic evolution of chondrites. *Earth and Planetary Science Letters*, 50(1), 139–155. [https://doi.org/10.1016/0012-821X\(80\)90125-9](https://doi.org/10.1016/0012-821X(80)90125-9)
- Jakubowicz, M., Dopierska, J., & Belka, Z. (2015). Tracing the composition and origin of fluids at an ancient hydrocarbon seep (Hollard Mound, Middle Devonian, Morocco): A Nd, REE and stable isotope study. *Geochimica et Cosmochimica Acta*, 156, 50–74. <https://doi.org/10.1016/j.gca.2015.02.027>
- Jansa, L., Gardner, J. V., & Dean, W. E. (1978). *Mesozoic sequences of the Central North Atlantic* (Initial Reports of the Deep Sea Drilling Project). <https://doi.org/10.2973/dsdp.proc.41.138.1978>
- Key, R. M., Loughlin, S. C., Gillespie, M., Del Rio, M., Horstwood, M. S. A., Crowley, Q. G., et al. (2008). Two Mesoarchaean terranes in the Reguibat shield of NW Mauritania. *Geological Society, Special Publications*, 297(1), 33–52. <https://doi.org/10.1144/SP297.3>
- Klitgord, K., & Schouten, S. (1986). Plate kinematics of the central Atlantic. In *The Geology of North America* (Vol. 1000, pp. 351–378).
- Kouamelan, A. N., Delor, C., & Peucat, J. J. (1997). Geochronological evidence for reworking of Archean terrains during the early Proterozoic (2.1 Ga) in the western Cote d'Ivoire (Man Rise–West African Craton). *Precambrian Research*, 86(3–4), 177–199. [https://doi.org/10.1016/S0301-9268\(97\)00043-0](https://doi.org/10.1016/S0301-9268(97)00043-0)
- Labails, C., Olivet, J.-L., Aslanian, D., & Roest, W. R. (2010). An alternative early opening scenario for the Central Atlantic Ocean. *Earth and Planetary Science Letters*, 297(3–4), 355–368. <https://doi.org/10.1016/j.epsl.2010.06.024>
- Lacan, F. (2002). *Masses d'eau des Mers Nordiques et de l'Atlantique Subarctique tracées par les isotopes du néodyme* (doctoral dissertation). Université Paul Sabatier-Toulouse III. <https://doi.org/10.1.1.633.7605>
- Lancelot, Y., Seibold, E., Cepek, P., Dean, W. E., Eremeev, V., Gardner, J. V., et al. (1978). Site 367: *Cape Verde Basin* (Initial Reports of the Deep Sea Drilling Project 41, pp. 163–232). <https://doi.org/10.2973/dsdp.proc.41.103.1978>

- Lancelot, Y., & Winterer, E. L. (1980). *Introduction and Summary of Results, Deep Sea Drilling Project Leg 50* (Initial Reports of the Deep Sea Drilling Project 50, pp. 5–11). <https://doi.org/10.2973/dsdp.proc.50.101.1980>
- Latil-Brun, M. V., & Lucazeau, F. (1988). Subsidence, extension and thermal history of the West African margin in Senegal. *Earth and Planetary Science Letters*, 90(2), 204–220. [https://doi.org/10.1016/0012-821X\(88\)90101-X](https://doi.org/10.1016/0012-821X(88)90101-X)
- Ledru, P., Johan, V., Milési, J. P., & Tegye, M. (1994). Markers of the last stages of the Palaeoproterozoic collision: Evidence for a 2 Ga continent involving circum-South Atlantic provinces. *Precambrian Research*, 69(1–4), 169–191. [https://doi.org/10.1016/0301-9268\(94\)90085-X](https://doi.org/10.1016/0301-9268(94)90085-X)
- Le Goff, É., Guerrot, C., Maurin, G., Johan, V., Tegye, M., & Zerga, M. B. (2001). Découverte d'éclotites hercyniennes dans la chaîne septentrionale des Mauritanides (Afrique de l'Ouest). *Comptes Rendus de l'Académie des Sciences-Series IIA-Earth and Planetary Science*, 333(11), 711–718. [https://doi.org/10.1016/S1251-8050\(01\)01694-9](https://doi.org/10.1016/S1251-8050(01)01694-9)
- Le Pichon, X. (1968). Sea-floor spreading and continental drift. *Journal of Geophysical Research*, 73(12), 3661–3697. <https://doi.org/10.1029/JB073i012p03661>
- Leprêtre, R., Missenard, Y., Barbarand, J., Gautheron, C., Saddiqi, O., & Pinna-Jamme, R. (2015). Postrift history of the eastern central Atlantic passive margin: Insights from the Saharan region of South Morocco. *Journal of Geophysical Research: Solid Earth*, 120, 4645–4666. <https://doi.org/10.1002/2014JB011549>
- Martin, E. E., Blair, S. W., Kamenov, G. D., Scher, H. D., Bourbon, E., Basak, C., et al. (2010). Extraction of Nd isotopes from bulk deep sea sediments for paleoceanographic studies on Cenozoic time scales. *Chemical Geology*, 269(3–4), 414–431. <https://doi.org/10.1016/j.chemgeo.2009.10.016>
- Martin, E. E., MacLeod, K. G., Jiménez Berrocoso, A., & Bourbon, E. (2012). Water mass circulation on Demerara Rise during the Late Cretaceous based on Nd isotopes. *Earth and Planetary Science Letters*, 327–328, 111–120. <https://doi.org/10.1016/j.epsl.2012.01.037>
- Marzoli, A., Melluso, L., Morra, V., Renne, P. R., Sgroso, I., D'Antonio, M., et al. (1999). Geochronology and petrology of Cretaceous basaltic magmatism in the Kwanza basin (western Angola), and relationships with the Paranà-Etendeka continental flood basalt province. *Journal of Geodynamics*, 28(4–5), 341–356. [https://doi.org/10.1016/S0264-3707\(99\)00014-9](https://doi.org/10.1016/S0264-3707(99)00014-9)
- McLennan, S. M., Hemming, S., McDaniel, D. K., & Hanson, G. N. (1993). Geochemical approaches to sedimentation, provenance, and tectonics. *Geological Society of America Special Papers*, 284, 21–40. <https://doi.org/10.1130/SPE284-p21>
- Meyer, I., Davies, G. R., & Stuut, J.-B. W. (2011). Grain size control on Sr-Nd isotope provenance studies and impact on paleoclimate reconstructions: An example from deep-sea sediments offshore NW Africa. *Geochemistry, Geophysics, Geosystems*, 12, Q03005. <https://doi.org/10.1029/2010GC003355>
- Milesi, J.-P., Frizon de Lamotte, D., UNESCO. (2010). *Carte tectonique de l'Afrique: Tectonic map of Africa*. CCGM/UNESCO.
- Mohammed, T., Jean-Yves, C., Peter, B., Christophe, R. (2015). Petrogenesis of the post-collisional Bled M'Dena volcanic ring complex in Reguibat Rise (western Eglab shield, Algeria). *Journal of African Earth Sciences*. Retrieved from <http://www.sciencedirect.com/science/article/pii/S1464343X1500076X>; <https://doi.org/10.1016/j.jafrearsci.2015.04.003>
- Moiroud, M., Pucéat, E., Donnadieu, Y., Bayon, G., Guiraud, M., Voigt, S., et al. (2016). Evolution of neodymium isotopic signature of seawater during the Late Cretaceous: Implications for intermediate and deep circulation. *Gondwana Research*, 36, 503–522. <https://doi.org/10.1016/j.gr.2015.08.005>
- Montero, P., Haissen, F., El Archi, A., Rjmati, E., & Bea, F. (2014). Timing of Archean crust formation and cratonization in the Awsard-Tichla zone of the NW Reguibat Rise, West African Craton: A SHRIMP, Nd–Sr isotopes, and geochemical reconnaissance study. *Precambrian Research*, 242, 112–137. <https://doi.org/10.1016/j.precamres.2013.12.013>
- Moulin, M., Aslanian, D., & Unternehr, P. (2010). A new starting point for the South and Equatorial Atlantic Ocean. *Earth-Science Reviews*, 98(1–2), 1–37. <https://doi.org/10.1016/j.earscirev.2009.08.001>
- Nesbitt, H. W., & Young, G. M. (1982). Early Proterozoic climates and plate motions inferred from major element chemistry of lutites. *Nature*, 299(5885), 715–717. <https://doi.org/10.1038/299715a0>
- Olivet, J. L., Bonnin, J., Beuzart, P., & Auzende, J.-M. (1984). Cinématique de l'Atlantique Nord et Central. *Publications du C.N.E.X.O. Série Rapports scientifiques et techniques*, 54, 1–108.
- Olsen, P. E. (1999). Giant lava flows, mass extinctions, and mantle plumes. *Science*, 284(5414), 604–605. <https://doi.org/10.1126/science.284.5414.604>
- Othman, D. B., Polvé, M., & Allègre, C. J. (1984). Nd–Sr isotopic composition of granulites and constraints on the evolution of the lower continental crust. *Nature*, 307(5951), 510–515. <https://doi.org/10.1038/307510a0>
- Patchett, P. J., Ross, G. M., & Gleason, J. D. (1999). Continental drainage in North America during the phanerozoic from Nd isotopes. *Science*, 283(5402), 671–673. <https://doi.org/10.1126/science.283.5402.671>
- Pawlig, S., Gueye, M., Klischies, R., Schwarz, S., Wemmer, K., & Siegesmund, S. (2006). Geochemical and Sr–Nd isotopic data on the Birimian of the Kedougou-Kenieba inlier (Eastern Senegal): Implications on the Palaeoproterozoic evolution of the West African Craton. *South African Journal of Geology*, 109(3), 411–427. <https://doi.org/10.2113/jgsajg.109.3.411>
- Peucat, J. J., Capdevila, R., Drareni, A., Mahdjoub, Y., & Kahoui, M. (2005). The Eglab massif in the West African Craton (Algeria), an original segment of the Eburnean orogenic belt: Petrology, geochemistry and geochronology. *Precambrian Research*, 136(3–4), 309–352. <https://doi.org/10.1016/j.precamres.2004.12.002>
- Pflaumann, U., & Čepe, P. (1982). Cretaceous foraminiferal and nannoplankton biostratigraphy and paleoecology along the West African continental margin. In *Geology of the Northwest African continental margin* (pp. 309–353). https://doi.org/10.1007/978-3-642-68409-8_13
- Piper, D. Z. (1974). Rare earth elements in ferromanganese nodules and other marine phases. *Geochimica et Cosmochimica Acta*, 38(7), 1007–1022. [https://doi.org/10.1016/0016-7037\(74\)90002-7](https://doi.org/10.1016/0016-7037(74)90002-7)
- Pletsch, T., Chamley, H., Daoudi, L., Deconinck, J. F., & Charroud, M. (1996). Palaeogeographic controls on palygorskite occurrence in mid-Cretaceous sediments of Morocco and adjacent basins. *Clay Minerals*, 31(3), 403–416. <https://doi.org/10.1180/claymin.1996.031.3.10>
- Potrel, A., Peucat, J. J., & Fanning, C. M. (1998). Archean crustal evolution of the West African Craton: Example of the Amsaga Area (Reguibat Rise). U–Pb and Sm–Nd evidence for crustal growth and recycling. *Precambrian Research*, 90(3–4), 107–117. [https://doi.org/10.1016/S0301-9268\(98\)00044-8](https://doi.org/10.1016/S0301-9268(98)00044-8)
- Poulsen, C. J., Barron, E. J., Arthur, M. A., & Peterson, W. H. (2001). Response of the mid-Cretaceous global oceanic circulation to tectonic and CO₂ forcings. *Palaeoceanography*, 16(6), 576–592. <https://doi.org/10.1029/2000PA000579>
- Pucéat, E., Lécuyer, C., & Reisberg, L. (2005). Neodymium isotope evolution of NW Tethyan upper ocean waters throughout the Cretaceous. *Earth and Planetary Science Letters*, 236, 705–720. <https://doi.org/10.1016/j.epsl.2005.03.015>
- Robinson, S. A., & Vance, D. (2012). Widespread and synchronous change in deep-ocean circulation in the North and South Atlantic during the Late Cretaceous. *Palaeoceanography*, 27, PA1102. <https://doi.org/10.1029/2011PA002240>
- Roddaz, M., Debat, P., & Nikiéma, S. (2007). Geochemistry of Upper Birimian sediments (major and trace elements and Nd–Sr isotopes) and implications for weathering and tectonic setting of the Late Paleoproterozoic crust. *Precambrian Research*, 159(3–4), 197–211. <https://doi.org/10.1016/j.precamres.2007.06.008>

- Roddaz, M., Viers, J., Moreira-Turcq, P., Blondel, C., Sondag, F., Guyot, J.-L., et al. (2014). Evidence for the control of the geochemistry of Amazonian floodplain sediments by stratification of suspended sediments in the Amazon. *Chemical Geology*, 387, 101–110. <https://doi.org/10.1016/j.chemgeo.2014.07.022>
- Rosenbaum, G., Lister, G. S., & Duboz, C. (2002). Relative motions of Africa, Iberia and Europe during Alpine orogeny. *Tectonophysics*, 359(1–2), 117–129. [https://doi.org/10.1016/S0040-1951\(02\)00442-0](https://doi.org/10.1016/S0040-1951(02)00442-0)
- Samson, S. D., Inglis, J. D., D'Lemos, R. S., Admou, H., Blichert-Toft, J., & Hefferan, K. (2004). Geochronological, geochemical, and Nd–Hf isotopic constraints on the origin of Neoproterozoic plagiogranites in the Tasriwine ophiolite, Anti-Atlas orogen, Morocco. *Precambrian Research*, 135(1–2), 133–147. <https://doi.org/10.1016/j.precamres.2004.08.003>
- Schaltegger, U., Stille, P., Rais, N., Piqué, A., & Clauer, N. (1994). Neodymium and strontium isotopic dating of diagenesis and low-grade metamorphism of argillaceous sediments. *Geochimica et Cosmochimica Acta*, 58(5), 1471–1481. [https://doi.org/10.1016/0016-7037\(94\)90550-9](https://doi.org/10.1016/0016-7037(94)90550-9)
- Schlanger, S., & Jenkyns, H. (1976). Cretaceous oceanic anoxic events: Causes and consequences. *Geologie en Mijnbouw*, 55, 179–184.
- Schoepfer, S. D., Shen, J., Wei, H., Tyson, R. V., Ingall, E., & Algeo, T. J. (2015). Total organic carbon, organic phosphorus, and biogenic barium fluxes as proxies for paleomarine productivity. *Earth-Science Reviews*, 149, 23–52. <https://doi.org/10.1016/j.earscirev.2014.08.017>
- Scotese, C. R., & Golonka, J. (1997). *Paleogeographic Atlas* (pp. 1–45). PALEOMAP Project, University of Texas at Arlington.
- Sengör, A. M. C., & Burke, K. (1978). Relative timing of rifting and volcanism on Earth and its tectonic implications. *Geophysical Research Letters*, 5(6), 419–421. <https://doi.org/10.1029/GL005i006p00419>
- Shirey, S. B., & Richardson, S. H. (2011). Start of the Wilson cycle at 3 Ga shown by diamonds from subcontinental mantle. *Science*, 333(6041), 434–436. <https://doi.org/10.1126/science.1206275>
- Sibuet, J.-C., & Mascle, J. (1978). Plate kinematic implications of Atlantic equatorial fracture zone trends. *Journal of Geophysical Research*, 83(B7), 3401–3421. <https://doi.org/10.1029/JB083iB07p03401>
- Soumaila, A., Henry, P., Garba, Z., & Rossi, M. (2008). REE patterns, Nd–Sm and U–Pb ages of the metamorphic rocks of the Diagorou–Darbani greenstone belt (Liptako, SW Niger): Implication for Birimian (Palaeoproterozoic) crustal genesis. *Geological Society, Special Publications*, 297(1), 19–32. <https://doi.org/10.1144/SP297.2>
- Tahiri, A., Montero, P., El Hadi, H., Poyatos, D. M., Azor, A., Bea, F., et al. (2010). Geochronological data on the Rabat–Tiflet granitoids: Their bearing on the tectonics of the Moroccan Variscides. *Journal of African Earth Sciences*, 57(1–2), 1–13. <https://doi.org/10.1016/j.jafrearsci.2009.07.005>
- Taylor, P. N., Moorbath, S., Leube, A., & Hirdes, W. (1992). Early Proterozoic crustal evolution in the Birimian of Ghana: Constraints from geochronology and isotope geochemistry. *Precambrian Research*, 56(1–2), 97–111. [https://doi.org/10.1016/0301-9268\(92\)90086-4](https://doi.org/10.1016/0301-9268(92)90086-4)
- Taylor, S. R., & McLennan, S. M. (1985). *The continental crust: Its composition and evolution*. Oxford, UK: Blackwell Scientific Publications.
- Thomas, R. J., Chevallier, L. P., Gresse, P. G., Harmer, R. E., Eglington, B. M., Armstrong, R. A., et al. (2002). Precambrian evolution of the Sirwa Window, Anti-Atlas Orogen, Morocco. *Precambrian Research*, 118(1–2), 1–57. [https://doi.org/10.1016/S0301-9268\(02\)00075-X](https://doi.org/10.1016/S0301-9268(02)00075-X)
- Torsvik, T. H., & Cocks, L. R. M. (2013). Gondwana from top to base in space and time. *Gondwana Research*, 24(3–4), 999–1030. <https://doi.org/10.1016/j.gr.2013.06.012>
- Torsvik, T. H., Müller, R. D., Van der Voo, R., Steinberger, B., & Gaina, C. (2008). Global plate motion frames: Toward a unified model. *Reviews of Geophysics*, 46, RG3004. <https://doi.org/10.1029/2007RG000227>
- Torsvik, T. H., Van der Voo, R., Preeden, U., Mac Niocaill, C., Steinberger, B., Doubrovine, P. V., et al. (2012). Phanerozoic polar wander, palaeogeography and dynamics. *Earth-Science Reviews*, 114(3–4), 325–368. <https://doi.org/10.1016/j.earscirev.2012.06.007>
- Toummite, A., Liégeois, J. P., Gasquet, D., Bruguier, O., Beraaouz, E. H., & Ikenne, M. (2013). Field, geochemistry and Sr–Nd isotopes of the Pan-African granitoids from the Tifnoute Valley (Sirwa, Anti-Atlas, Morocco): A post-collisional event in a metacratonic setting. *Mineralogy and Petrology*, 107(5), 739–763. <https://doi.org/10.1007/s00710-012-0245-3>
- Trabucho Alexandre, J., Tuentner, E., Henstra, G. A., van der Zwan, K. J., van de Wal, R. S., Dijkstra, H. A., et al. (2010). The mid-Cretaceous North Atlantic nutrient trap: Black shales and OAEs. *Palaeogeography*, 25, PA4201. <https://doi.org/10.1029/2010PA001925>
- Valentine, J. W., & Moores, E. M. (1970). Plate-tectonic regulation of faunal diversity and sea level: A model. *Nature*, 228(5272), 657–659. <https://doi.org/10.1038/228657a0>
- Verati, C., Bertrand, H., & Féraud, G. (2005). The farthest record of the Central Atlantic Magmatic Province into West Africa craton: Precise $^{40}\text{Ar}/^{39}\text{Ar}$ dating and geochemistry of Taoudenni basin intrusives (northern Mali). *Earth and Planetary Science Letters*, 235(1–2), 391–407. <https://doi.org/10.1016/j.epsl.2005.04.012>
- Viers, J., Roddaz, M., N., F., Jr., Guyot, J.-L., Sondag, F., Brunet, P., Zouiten, C., et al. (2008). Seasonal and provenance controls on Nd–Sr isotopic compositions of Amazon Rivers suspended sediments and implications for Nd and Sr fluxes exported to the Atlantic Ocean. *Earth and Planetary Science Letters*, 274(3–4), 511–523. <https://doi.org/10.1016/j.epsl.2008.08.011>
- Villeneuve, M., & Cornée, J. J. (1994). Structure, evolution and palaeogeography of the West African Craton and bordering belts during the Neoproterozoic. *Precambrian Research*, 69(1–4), 307–326. [https://doi.org/10.1016/0301-9268\(94\)90094-9](https://doi.org/10.1016/0301-9268(94)90094-9)
- Villeneuve, M., Rochet, J., & Faye, M. (1993). Héritages structuraux panafricains et hercyniens sur la marge africaine de l’océan Atlantique, entre la Mauritanie et le Liberia. *Bulletin de la Société Géologique de France*, 164, 851–860.
- Voigt, S., Jung, C., Friedrich, O., Frank, M., Teschner, C., & Hoffmann, J. (2013). Tectonically restricted deep-ocean circulation at the end of the Cretaceous greenhouse. *Earth and Planetary Science Letters*, 369–370, 169–177. <https://doi.org/10.1016/j.epsl.2013.03.019>
- Wegener, A. (1915). *Die Entstehung der Kontinente und Ozeane: Vieweg und Sohr., Braunschweig* (2nd ed., 1920; 3rd ed., 1922, translated into English in 1924; 4th ed., 1924, revised by A. Wegener and translated into English in 1929).
- Williams, G. L. (1978). *Palynological biostratigraphy, Deep Sea Drilling Project Sites 367 and 370* (Initial Reports of the Deep Sea Drilling Project). <https://doi.org/10.2973/dsdp.proc.38394041s.402.1978>
- Wilson, J. T. (1968). Static or mobile earth: The current scientific revolution. *Proceedings of the American Philosophical Society*, 112, 309–320.
- Zhao, G., Cawood, P. A., Wilde, S. A., & Sun, M. (2002). Review of global 2.1–1.8 Ga orogens: Implications for a pre-Rodinia supercontinent. *Earth-Science Reviews*, 59(1–4), 125–162. [https://doi.org/10.1016/S0012-8252\(02\)00073-9](https://doi.org/10.1016/S0012-8252(02)00073-9)